Nanoscale Advances

ROYAL SOCIETY OF CHEMISTRY

REVIEW

View Article Online
View Journal | View Issue

Check for updates

Cite this: *Nanoscale Adv.*, 2023, **5**, 3803

# A comprehensive review of the current progresses and material advances in perovskite solar cells

Rabia Sharif,[a] Arshi Khalid,[b] Syed Waqas Ahmad,[a] Abdul Rehman,[a] Haji Ghulam Qutab,[a] Hafiz Husnain Akhtar,[a] Khalid Mahmood,*[a] Shabana Afzal[c] and Faisal Saleem[a]

Recently, perovskite solar cells (PSCs) have attracted ample consideration from the photovoltaic community owing to their continually-increasing power conversion efficiency (PCE), viable solution-processed methods, and inexpensive materials ingredients. Over the past few years, the performance of perovskite-based devices has exceeded 25% due to superior perovskite films achieved using low-temperature synthesis procedures along with evolving appropriate interface and electrode-materials. The current review provides comprehensive knowledge to enhance the performance and materials advances for perovskite solar cells. The latest progress in terms of perovskite crystal structure, device construction, fabrication procedures, and challenges are thoroughly discussed. Also discussed are the different layers such as ETLs and buffer-layers employed in perovskite solar-cells, seeing their transmittance, carrier mobility, and band gap potentials in commercialization. Generally, this review delivers a critical assessment of the improvements, prospects, and trials of PSCs.

Received 11th May 2023
Accepted 20th June 2023

DOI: 10.1039/d3na00319a

rsc.li/nanoscale-advances

Open Access Article. Published on 02 1402. Downloaded on 14/11/1404 12:16:38 ..
This article is licensed under a Creative Commons Attribution-NonCommercial 3.0 Unported Licence.

## 1. Introduction

Energy deficiencies have caused a worldwide issue in the 21st century. At present, most of the biosphere's energy is produced from petroleum derivatives such as coal, oil, and natural gas; as per the US Energy Information Organization (EIA), in 2016, ~65% of power was produced from petroleum derivatives and ~20% was using thermal power, while just ~15% was from environmentally-friendly power pathways. The inclination to foster sustainable power innovations (such as wind, sun, hydroelectric and geothermal) to supplant the fossil fuel-based energy age has inspired significant logical studies. Among the diverse sustainable sources, sun-powered energy is one of the greatest encouraging advancements to fulfill the developing worldwide energy demands and to determine or moderate the ever-rising energy emergency because of the consumption of petroleum derivatives.[1]

Just 1% of energy creation was accounted for by the sun-based source as determined in 2013; sun-oriented power is probable to turn into the most critical wellspring of energy by 2050.[2] Sunlight-based energy enjoys a few critical upper hands over other sustainable technologies, in particular, the world-wide dispersion of daylight (conversely to wind, hydroelectric and geothermal assets that are contained to specific regions), the absence of unsafe waste generation (rather than thermal power), and the decentralized nature of sun-oriented energy age.[3]

Tackling renewable energy is obviously the arrangement to the world's taking off energy requests and the current world-wide environment emergency. Sun-oriented energy is the most bountiful renewable asset accessible on the earth.[4] Also, it is along these lines broadly contemplated by analysts across the globe. Photovoltaics have radically improved among the first and third ages, diminishing the cost of assembling, while at the same time keeping up with power effectiveness.[5]

Solar cells are viewed as a significant method for tackling environmental contamination issues and using sustainable power, so different kinds of solar cells have been created. Among them, the slight film solar cells, for example, perovskite solar cells (PSCs) and organic solar cells (OSCs) have drawn extraordinary consideration from analysts because of the benefits of basic assembly, lightweight, and arrangement handling. The certified most noteworthy PCE of single-junction PSCs and OSCs has reached 25.2 and 17.4%, respectively.[6]

Perovskite, named after the Russian mineralogist L. A. Perovski, has an explicit valuable stone construction with the $ABX_3$ formula (X = oxygen, halogen). The larger A cation occupies a cubo octahedral place common with twelve X anions, though the extra modest B cation is balanced out in an octahedral site imparted to six X anions. The most careful perovskites are

[a]*Department of Chemical & Polymer Engineering, University of Engineering & Technology Lahore, Faisalabad Campus, $3\frac{1}{2}$ Km. Khurrianwala – Makkuana By-Pass, Faisalabad, Pakistan. E-mail: khalid@uet.edu.pk*

[b]*Department of Humanities & Basic Sciences, University of Engineering & Technology Lahore, Faisalabad Campus, $3\frac{1}{2}$ Km. Khurrianwala – Makkuana By-Pass, Faisalabad, Pakistan*

[c]*Department of Basic Sciences, Humanities Muhammad Nawaz Shareef University of Engineering and Technology Multan, Pakistan*

© 2023 The Author(s). Published by the Royal Society of Chemistry

Open Access Article. Published on 02 1402. Downloaded on 14/11/1404 12:16:38 ..
This article is licensed under a Creative Commons Attribution-NonCommercial 3.0 Unported Licence.

oxides owing to their electrical characteristics of superconductivity or ferroelectricity. Halide perovskites attained less attention till coated organometal halide perovskites were testified to display semiconductor-to-metal development with growing dimensionality.[7]

The critical material for the PSCs as of late generating incredible consideration is the organometal halide $CH_3NH_3$-$MX_3$ (M = Pb or Sn, X = Cl, Br or I), whose construction and actual characteristics were primarily announced by Weber in 1978.[8] For $CH_3NH_3PbX_3$, there is an increment for the unit cell boundary from 5.68 to 5.92 and to 6.27 Å as the size of the halide goes from X = Cl to Br and to I. Lattice parameters in the cubic stage can be basically tuned by blending halides; for example, $CH_3NH_3PbBr_{2.3}C_{l0.7}$ presented $a$ = 5.98 Å, $CH_3NH_3PbBr_{2.07}I_{0.93}$ displayed $a$ = 6.03 Å, and $CH_3NH_3PbBr_{0.45}I_{2.55}$ exhibited $a$ = 6.25 Å. $CH_3NH_3SnBr_xI_{3-x}$ ($x$ = 0–3) crystalized to the cubic perovskite assembly with the unit cell parameters $a$ = 5.89 Å ($x$ = 3), $a$ = 6.01 Å ($x$ = 2) and $a$ = 6.24 Å ($x$ = 0). In spite of Pb-based perovskite materials, some Sn-based perovskite materials showed conducting characteristics.[9]

Organic–inorganic hybrid lead halide perovskites pulled in scientists' considerations during the 1970s and 1990s,[8,10] particularly for their remarkable conducting and semiconducting characteristics.[11] In 2009, the exploration endeavors to use lead perovskite as a light absorber in solar cells were reported by Miyasaka *et al.* consolidating $CH_3NH_3PbI_3$ ($MAPbI_3$) and $CH_3NH_3PbBr_3$ ($MAPbBr_3$) as sensitizers into color sharpened solar cells (DSSCs), demonstrating 3.8 and 3.1% PCE, respectively.[12]

Considering the significant source of perfect and feasible energy on the planet, solar flux has for some time been looked to change over into power over the photovoltaic impact of light-retaining semiconductors. Prior age photovoltaics used inorganic translucent semiconductors such as cadmium telluride (CdTe), silicon, and copper indium gallium selenide/sulfide (CIGS) as safeguards; these can be productive and steady, however, generally need high energy-input make, including and high-vacuum high-temperature methods.

The arising natural PSCs address one of the groundbreaking advancements since they are similar to OSCs;[13] furthermore, DSSCs, possibly can be fabricated into lightweight, adaptable, and minimal expense power causes through the high-throughput solution construction.[14] PSCs have subsequently obtained concentrated exploration endeavors from both the scholarly world and industry. The PCEs of PSCs have quickly improved from 3.8% to 22.1% in only seven years, showing the contention in productivity to that of silicon solar cells. It basically profits from the excellent optoelectrical characteristics of semiconducting natural inorganic hybrid perovskites, for example, the solid optical retention coefficient, an immediate band hole, long transporter life time and dispersion length,[15] and better electron/hole mobility in the crystalline stage.[15,16] More significantly, natural inorganic lead halide perovskites produce approximately reinforced exciton with minuscule holding energy, which works with the age of the free charge transporters inside the perovskite at the expense of insignificant driving force.[17] Subsequently, the fast headway of single intersection PSC has reached the level near its hypothetical effectiveness roof, through the consolidated advancements in the essential organization, glasslike film development, connection point and gadget engineering, and so forth.[18]

Although wonderful advances have been made for PSCs, various boundaries going from major to practical have actually remained, which should be further overcome to approve their business importance, as those of conventional silicon solar cells. For example, concerns on the functional steadiness of the PSC and naturally harmless perovskite organization should be additionally tended to for pushing PSC innovation for an enormous scope.[19,20] It is recognized that the $MAPbI_3$ perovskite can degrade under heat, moisture, and continued lighting in the air.[21] Along these lines, the model PSC has a generally short functional lifetime upon openness to dampness, hotness, and light. One essential for market thought is to broaden the life expectancy of PSCs prone to a very long time in open-air conditions. Then again, toxic perovskites comprise water-dissolvable Pb salt as a corruption item, which is poisonous upon human openness. Albeit these moves present obstructions to PSC progression, the reassuring disclosures have been accomplished in the new 2–3 years for PSCs. It presumably indicates that managing high-productivity and stable gadgets, as well as earth-harmless perovskites, are the basic, yet testing parts of PSC investigations. In this review, we center around the new developments of PSCs in the connected topics. In the accompanying pieces of this audit article, we initially present the methodologies that empower high-productivity PSCs through perovskite film handling, organization designing, interfacial layer, and pair engineering. Then, at that point, the material and gadget's secure qualities, and the improvement of perovskite without lead will be examined. In the last segment, we summarize along with brief viewpoints on further progressing PSC toward proficient and stable solar-to-power innovations.[22,23]

### 1.1. Arrangement of the perovskite crystal

Perovskites are called the most talented light-capturing solar cell materials for future photovoltaics. It was revealed in 1839 in the Ural Massifs in Russia and called after Russian mineralogist L. A. Perovski[24] for a perovskite with a chemical formula of $CaTiO_3$ (calcium titanium oxide). Complexes with analogous construction to $CaTiO_3$ ($ABX_3$) are named perovskites. Usually, in the $ABX_3$ construction (Fig. 1a), A is a huge monovalent cation with the cuboctahedral spots in a cubic site, B is a minor divalent metal cation lodging the octahedral positions, and X is an anion (characteristically a halogen; though, X may also be nitrogen, oxygen or carbon). However, when a halogen is located on anion sites in a perovskite assembly, as a consequence, there are monovalent and divalent cations in A and B positions, respectively.[25]

In order to enumerate the stability and structure of perovskites, two vital constraints are the octahedral factor ($\mu$) and tolerance factor ($t$)[26] The tolerance factor is defined as a ratio of the bond lengths of A–X and B–X in a perfect solid-sphere model. Scientifically, it can be written as:


© 2023 The Author(s). Published by the Royal Society of Chemistry

Open Access Article. Published on 02 1402. Downloaded on 14/11/1404 12:16:38 ..
This article is licensed under a Creative Commons Attribution-NonCommercial 3.0 Unported Licence.

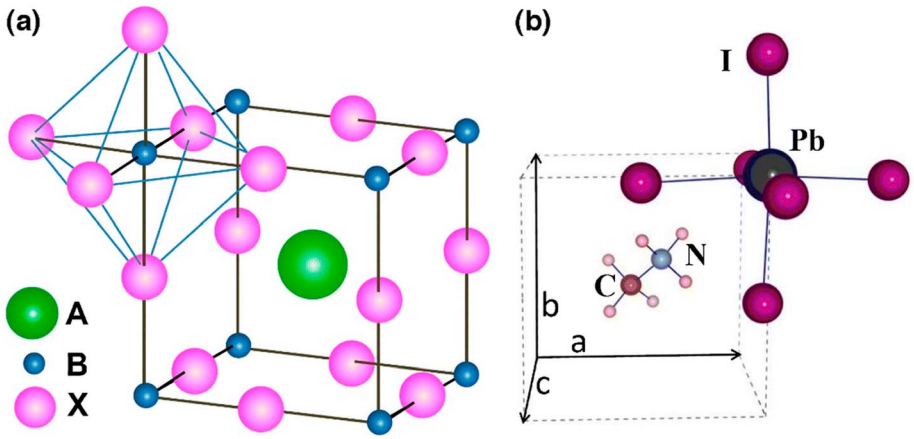


Fig. 1 (a) $ABX_3$ perovskite construction presenting $BX_6$ octahedral and bigger A cations engaged in the cuboctahedral place. (b) The element cell of cubic $MAPbI_3$ perovskite (reproduced with permission from ref. 25, copyright 2015 Elsevier).

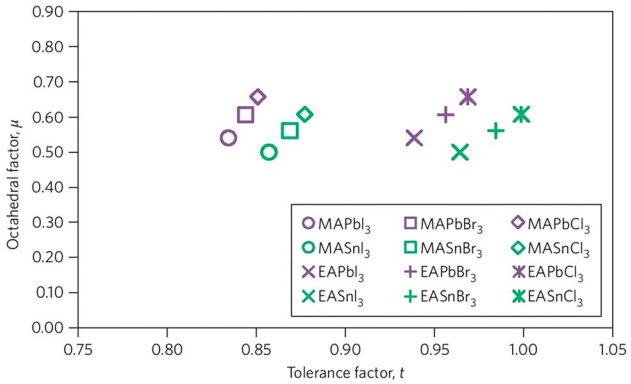


Fig. 2 Tolerance factor ($t$) and octahedral factor ($\mu$) calculated values for perovskites (reproduced with permission from ref. 28, copyright 2014 NPG).

$$t = \frac{(R_A + R_X)}{\sqrt{2}(R_B + R_X)}$$

where $R_A$, $R_B$, and $R_X$ denote the ionic radii of the A, B, and X, respectively.[27] On the other hand, $\mu$ is the ratio of the ionic radius of the divalent cation ($R_B$) and the radius of the anion (RX). Inferior values of $t$ results in fewer symmetric tetragonal or orthorhombic constructions, while large values of $t$ ($t > 1$) could weaken the 3D B–X system (Fig. 2).[28]

### 1.2. Working mechanism of PSCS

The working principles of OSCs and dye-sensitized solar cells (DSSCs) help in knowing the operation of PSCs. A representative diagram of the working mechanism of PSCs is shown in (Fig. 3). PSCs employ perovskite-structured light absorbers for photovoltaic motion; similarly, DSSCs use the dye/semiconductor boundary for light gathering. The photovoltaic structure has three key operative stages:

(1) Photon absorption trailed by the generation of free charge
(2) Transport of charge
(3) Extraction of charge

When sunlight strikes a PSC, the perovskite material grips light, excitons are formed, and charge transporters (electrons and holes) are formed upon exciton parting. Exciton parting occurs at the boundary between the charge-transporting layer and perovskite film. After the electron is detached from the hole and inserted into the electron transporting layer (ETL), it travels to the anode usually made of fluorine-doped tin oxide (FTO) glass. Instantaneously, the hole is inserted into the HTL and afterward travels to the cathode (typically a metal).[29] The holes and electrons are collected by counter and working electrodes, separately and moved to the outward circuit to generate current.[30,31]

### 1.3. Physical design of PSCs

Cell formation is a basic feature for assessing the complete role of solar cells. PSCs can be organized as usual (n–i–p) and inverted (p–i–n) constructions relying on which carrier (electron/hole) material is existing on the external side of the cell and that is met by incident light first. Further, these two

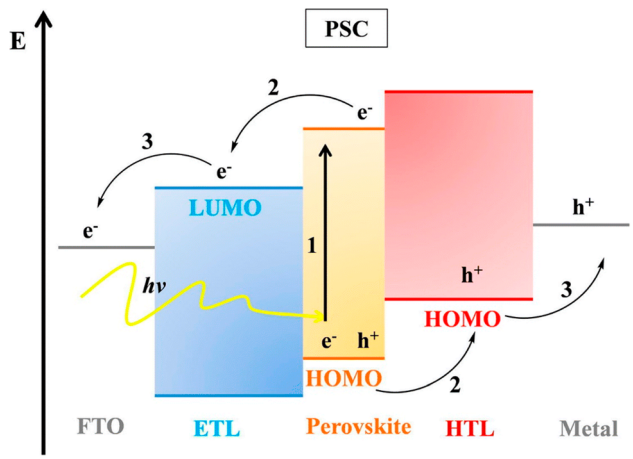


Fig. 3 Band plan and working mechanism of PSCs (reproduced with permission from ref. 32, copyright 2017 Elsevier).

Open Access Article. Published on 02 1402. Downloaded on 14/11/1404 12:16:38 ..
This article is licensed under a Creative Commons Attribution-NonCommercial 3.0 Unported Licence.

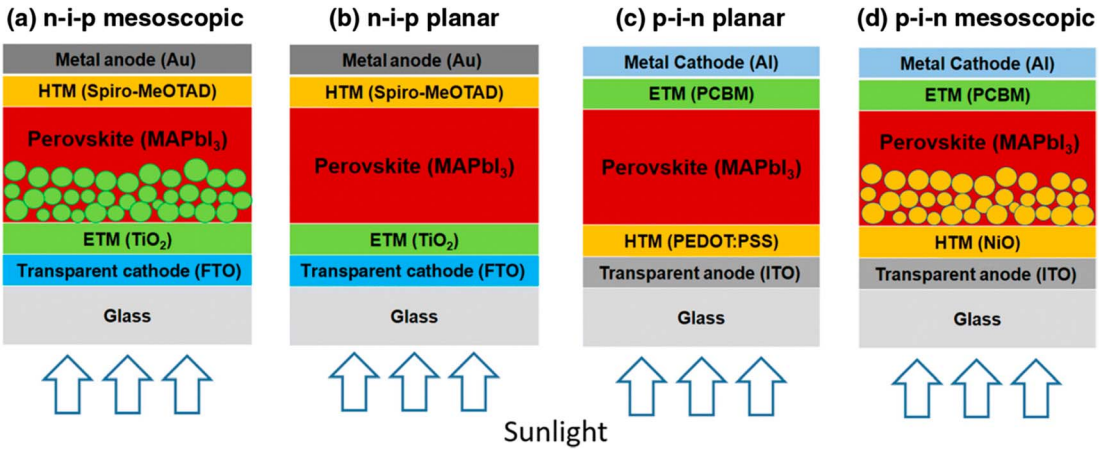


Fig. 4 Diagram displaying the four-layered assemblies of PSCs (a) n–i–p mesoscopic, (b) n–i–p planar, (c) p–i–n planar, and (d) p–i–n mesostructured (reproduced with permission from ref. 36, copyright 2016 SPIE).

assemblies can be categories as mesoscopic and planar cells. The perovskite devices based on mesoscopic construction include a mesoporous layer while the planar structure contains all planar films. Perovskite devices without holes and electron transporting layers have also been verified. In short, six categories of PSCs have been considered by several researchers so far: the mesoscopic n–i–p arrangement, planar n–i–p arrangement, planar p–i–n arrangement, mesoscopic p–i–n conformation, ETL-free structure, and HTL-free structure.

### 1.4. Classical n–i–p and inverted p–i–n formations

The regular n–i–p mesostructured construction was the first ever plan of perovskite devices to be verified, where the light-capturing dye was substituted with lead halide perovskite semiconductor materials in old-style DSSC-type cells.[32] The cells start with a transparent glass cathode trailed by the electron-transporting material (ETM).[33] The assembly is then covered using a mesostructured metal oxide comprising a perovskite absorber, trailed by the hole transport material (HTM), and topped with a metallic anode (Fig. 4a). This early progress for perovskite devices formed a significant area of research for the photovoltaic community and therefore directed to the growth of other perovskite device arrangements (Fig. 4b–d). It is imaginable to attain better performance in the absence of mesoporous film by wisely monitoring the boundaries between the various layers that construct the planner PSC.[34,35]

Using the identical materials and method, a planar n–i–p PSC displays improved open-circuit voltage ($V_{OC}$) and short-circuit current density ($J_{SC}$) compared to mesostructured PSCs, but, the planar devices showed more *J–V* hysteresis, which was a big question about the testified efficiencies.[36] The depth and grain of this buffer film mainly affect the *J–V* hysteresis curves.[37] Kim *et al.* detected that the negligible hysteresis in *J–V* curves was found by reducing the capacitance, which was accomplished by substituting Spiro-OMeTAD with poly(3,4-ethylenedioxythiophene)-poly(styrene sulfonate) (PEDOT:PSS).[38] Though, the behavior of *J–V* hysteresis also relies on the scan direction of voltage, scan range, and rate.[39] In order to overcome this issue, a slim mesoporous buffer coating was combined inside the planar n–i–p PSC assembly. Though mesoporous PSC displayed improved performance compared to planar devices, it is essential to produce a slim mesoporous film (less than 300 nm). Moreover, the planar device could be made-up using a low-temperature method in contrast with the mesostructured cells. However, the improved formation of the perovskite-absorbing film is essential.[40,41]

The p–i–n structured-based perovskite devices are based on organic solar cells.[42] In this case, the HTM layer is first coated before the ETL is formed. It was revealed that perovskites are proficient enough to transfer the holes themselves,[43] which was helpful to introduce the initial planar hetero-junction PSC having an inverted operational assembly.[36] With this development, the inverted p–i–n conformation has extended the possibilities to discover further selective layers from organic to inorganic materials. Planar p–i–n PSC facilitates their processing at low-temperature, slight *J–V* hysteresis having a high PCE of 18%.[44,45] The device arrangement of the inverted mesoscopic and planar p–i–n PSCs is revealed in Fig. 4c and d.

In addition, inexpensive HTM-free carbon-based PSCs (C-PSCs) have attracted significant attention because of their superior stability, and ease of fabrication, which make them highly suitable to replace HTL and metal electrodes. Zhiliang *et al.*, first described high-temperature treated mesostructured support designed ($TiO_2$/$ZrO_2$/C) HTL-free C-PSCs,[226] which confirmed effectual charge transference at perovskite/carbon and $TiO_2$/perovskite boundaries. With the hard work of scientists, the PCE of these devices has surpassed 17%.[227] In the recent past, planar-designed HTL-free C-PSCs utilized low-temperature treated tin oxide ($SnO_2$) (150 °C) to substitute $TiO_2$ as an ETL and have been established as an alternate cell assembly,[228] though, the inadequate interfacial charge transfer strictly bounds the performance of these devices. Thus, interfacial charge transfer strengthening is vital for high-performance planar-organized HTL-free C-PSCs. Many efforts


© 2023 The Author(s). Published by the Royal Society of Chemistry

Open Access Article. Published on 02 1402. Downloaded on 14/11/1404 12:16:38 ..
This article is licensed under a Creative Commons Attribution-NonCommercial 3.0 Unported Licence.

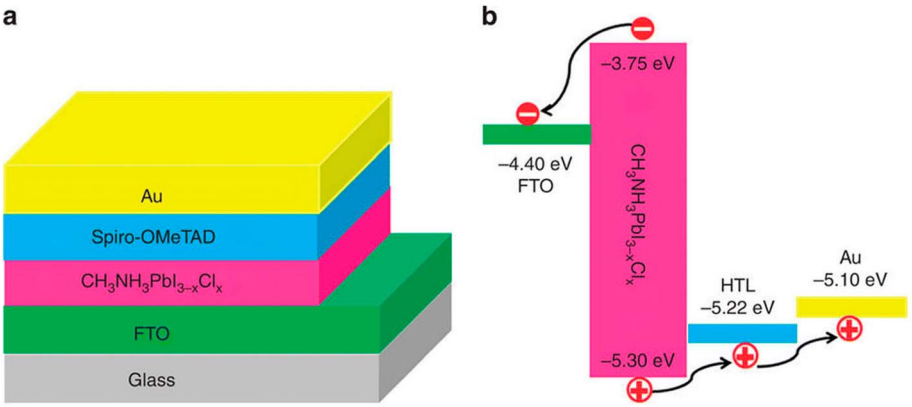


Fig. 5 (a) Symbolic representation of the ETL-free planar PSC arrangement and (b) energy level illustration of the planar PSC presenting gathering and parting of photo-generated electrons and holes in the absence of ETL (reproduced with permission from ref. 48, copyright 2015 NPG).

have been put into advancing the interaction at the perovskite/carbon boundary using either inserting carbon nanotubes as bonds or presenting nanosized carbon materials to block the openings at the perovskite/carbon border.[229,230]

### 1.5. ETL-free perovskite devices

A dense layer of metal oxide on the surface of transparent conductive oxide (TCO) is constantly essential for classical planar PSCs since it aids to attain high $V_{OC}$ and overall device performance. However, Huang *et al.* established a surface amendment method by applying a cesium salt solution to amend the surface of indium-tin-oxide (ITO) or to adjust the energy level arrangement at the interface, which directed to a PCE of 15.1%.[46] Further, compact layer-free perovskite devices were developed by the researchers, which showed 13.5% PCE by straight coating the perovskite absorber layer onto the ITO with the help of a sequential layer deposition technique, indicating that the presence of ETL is not essential to gain better device performances.[47] Ke *et al.* also recommended that a $TiO_2$ ETL may not be a perfect interfacial material after producing an effective ETL-free PSC producing a PCE of 14.14% rightly coated on an FTO glass substrate using a one-step method with no hole-blocking films.[48] The dense ETM layer-free planar PSC construction is displayed in Fig. 5. Other researchers have also shown that the compact layer-free style can produce admirable cell efficiency when made using various layer-processing procedures.[49]

### 1.6. HTL-free PSCs

Though numerous hole transport materials (HTMs) were introduced with decent consequences (namely inorganic compounds, polymers, and small molecules), HTM-free PSC designs are a modest cell arrangement. This increasing importance is due to the testified highly effective PSCs

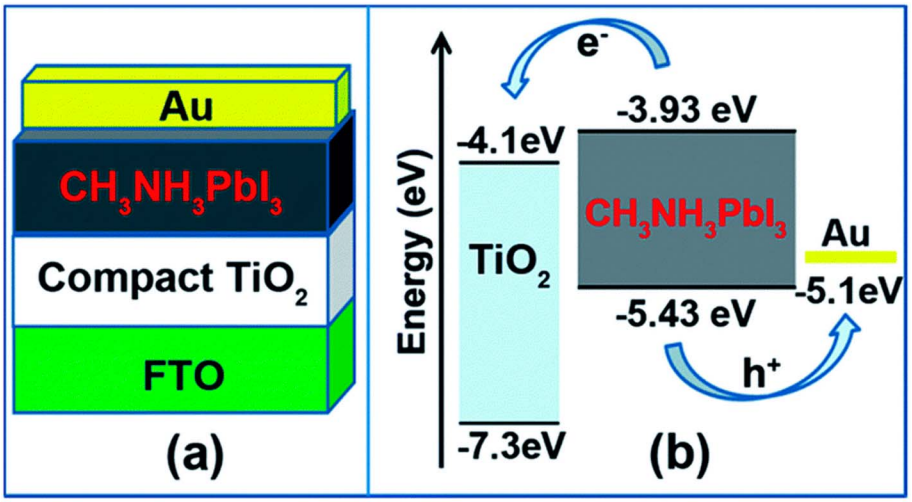


Fig. 6 Simplified model of the (a) construction and (b) energy level arrangement of the planar HTL-free PSCs (reproduced with permission from ref. 53, copyright 2016 Elsevier).

Open Access Article. Published on 02 1402. Downloaded on 14/11/1404 12:16:38 ..
This article is licensed under a Creative Commons Attribution-NonCommercial 3.0 Unported Licence.

comprising exclusive HTMs such as fullerenes, which meaningfully surge the manufacturing cost of these cells. As previously stated, perovskite materials expressed excellent semiconducting characteristics such as ambipolar behavior and longer lifetimes of charge transport, which eliminated the use of HTL.[50] For the first time ever, Etgar *et al.* suggested the fruitful manufacturing of HTL-free mesoscopic PSCs, demonstrating that $MAPbI_3$ itself worked both as a hole conductor and a light harvester.[44,51,52] The value of the perovskite absorber layer and the additional care of the performance of HTM-free PSCs. The simplest HTL-free PSC assembly is displayed in Fig. 6. The diverse cell conformations enlighten the choice of charge-transport (HTM and ETM) and charge-gathering materials (anode and cathode).

## 2. Types of materials for PSCs

### 2.1. Monovalent cation mixing/substitution

The alteration of monovalent cations can expand the efficiency of PSCs in a particular way. Though methylammonium lead iodide ($MAPbI_3$) is typically used as a light-absorbing material in perovskite devices; there is a continuing quest for other novel materials to substitute methylammonium (MA) in $MAPbI_3$ owing to their poor stability and insignificant band gap.[54] The optimum band gap in the case of single junction solar cells lies between 1.1 and 1.4 eV though the published band gaps of $MAPbI_3$ are between 1.50 and 1.61 eV.[55] Replacing the MA ion with a little bigger organic formamidinium (FA) ion consequences in a cubic assembly with a rather larger lattice and therefore a minor reduction in the band gap from 1.59 eV for $MAPbI_3$ to 1.45–1.52 eV for $FAPbI_3$ that permits collection of more light.[56] Similarly, Hanusch *et al.* disclosed that $FAPbI_3$ is thermally steadier than both $MAPbI_3$ and methylammonium lead bromide ($MAPbBr_3$), which sturdily proves the results that a bigger cation at the A site in $ABX_3$ assembly might support the perovskite structure in a better way.[57] Nevertheless, $FAPbI_3$ also has stability due to its sensitivity towards the contamination of solvent and humidity, since it results in photo-inactive, non-perovskite hexagonal δ-phase (yellow phase) or photoactive perovskite α-phase (black phase).[58,59] Fig. 7 displays the tolerance factor of steady alkali metals A = Rb, K, Li, Cs, and Na and two extra mutual monovalent cations MA and FA. The graphs of the tolerance factor represent that $MAPbI_3$, $FAPbI_3$, and $CsPbI_3$ lie in the range of 0.8 to 1.0 having a black phase. It was also observed that on heating $CsPbI_3$, the layer goes black while $RbPbI_3$ stays yellow. Therefore, in spite of its outstanding oxidation constancy, alone Rb may not be utilized in perovskite devices.[60]

In the recent past, Prochowicz *et al.* verified that the inclusion of 25 molar% of MAI to the reaction blend may steady the black stage of $FAPbI_3$, and they achieved a PCE of 14.98% having a $J_{SC}$ of 23.7 mA $cm^{-2}$.[49,62] Choi *et al.* described that doping the $MAPbI_3$ structure with 10% Cs gave rise to a 40% improvement in device productivity due to better morphology and enhanced light absorption.[63] Lee *et al.* established that moisture and photo-stability of $FA_{0.9}Cs_{0.1}PbI_3$ were considerably enhanced compared to pristine $FAPbI_3$.[54,64] Keeping in mind the target of high device performance and long-term stability, Cs was adopted to explore more complex cation combinations, *i.e.*, Cs/MA/FA. The triple-cation (Cs/MA/FA)-based PSCs have duplicability and thermal constancy than MA/FA double-cation perovskites.[60] The addition of Cs into MA/FA cation blends aids to disintegrate the cubic $PbI_2$ and photo-sluggish hexagonal δ-phase of $FAPbI_3$ totally. Additionally, the addition of Cs in different quantities (5%, 10%, 15%) caused a blue shift of 10 nm for the photoluminescence (PL) and absorption spectra along with a smaller cationic radius, creating the black perovskite stage extra intrinsically steady even at room temperature.[60] These findings are displayed in Fig. 8.

In order to discover other monovalent cations, Saliba *et al.* fused Rb into a photoactive perovskite phase by introducing various cation (RbCsMAFA) designs. Alkali metals were chosen

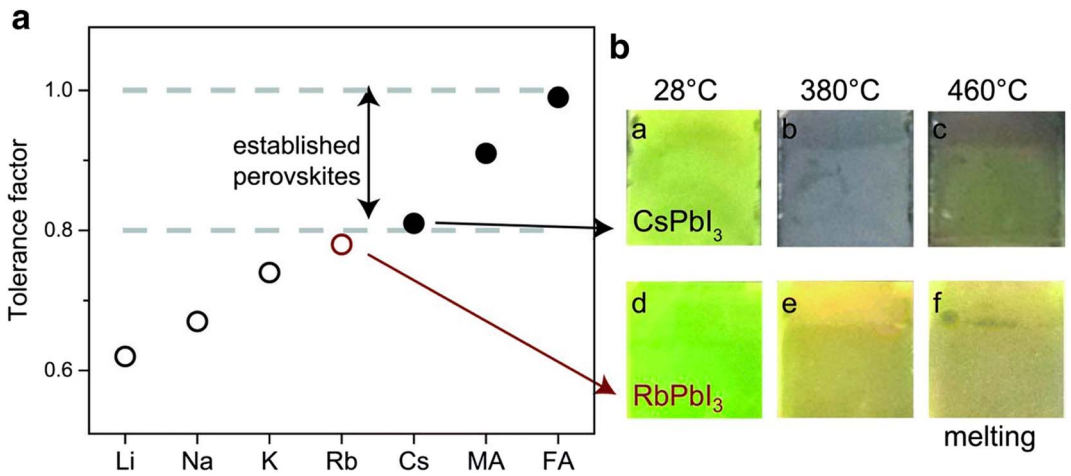


Fig. 7 Tolerance factor and perovskite pictures at diverse temperatures. The tolerance factor of perovskite between 0.8 to 1.0 displays a photoactive black stage (solid circles) whereas a tolerance factor below 0.8 shows a non-photoactive stage (open circles). Reproduced with permission from ref. 61. Copyright 2016 AAAS.


© 2023 The Author(s). Published by the Royal Society of Chemistry

Open Access Article. Published on 02 1402. Downloaded on 14/11/1404 12:16:38 ..
This article is licensed under a Creative Commons Attribution-NonCommercial 3.0 Unported Licence.

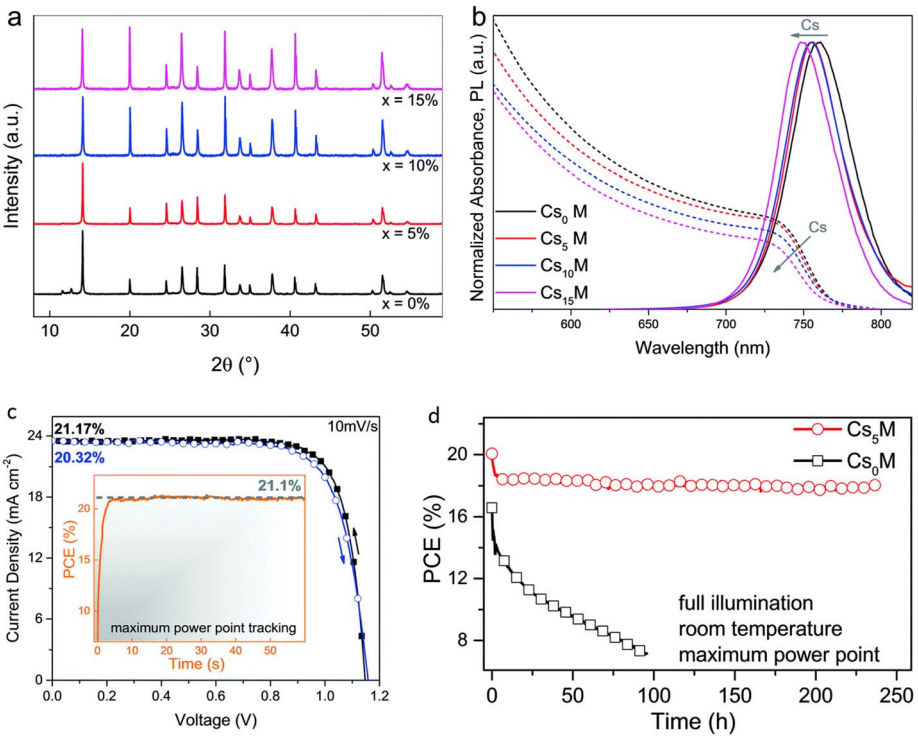


Fig. 8 Consequences of Cs accumulation in MA/FA cation blends; (a) XRD and (b) optical findings (c) current–voltage (*J*–*V*) and (d) stability properties of $Cs_x$MAFA complexes (reproduced with permission from ref. 60. Copyright 2017 RSC).

as the monovalent cations owing to their intrinsic stability in the oxidation environment. They also recognized various combinations of cationic perovskites such as RbCsFA, RbCsMAFA, RbFA, and RbMAFA producing reliable device efficiency as compared to formerly discovered cationic mixture-based perovskites such as CsMAFA and CsFA. These findings unlocked the access to utilize other organic–inorganic cation mixtures together with further inorganic cations in perovskite devices.[61]

### 2.2. Halide substitution

The substitution or replacement of halogen ions may adjust the optoelectronic characteristics of perovskite materials. In the $MAPbI_3$ assembly, iodine(I) can be replaced with both bromine and chlorine, and huge single crystals were formed using all three lead halide perovskites; $MAPbI_3$, $MAPbCl_3$, and $MAPbBr_3$ (Fig. 9). Liu *et al.* evaluated the optical characteristics (PL spectra, band gap, and absorption spectra) of $MAPbX_3$ (X = Cl, Br, I) as a function of the halogen anions, as displayed in Fig. 10. A sudden change in the absorbance was observed after the halide was replaced with Br, Cl, and I. As the ionic radius of the halide increases, the band gap energy reduces, such as for a single crystal, the band gap is 2.97, 2.24, and 1.53 eV for the Cl, Br, and I perovskite, respectively. Furthermore, the reduced PL peak intensities compared to the absorption onsets make it ideal for them to be used in solar cells.[64,65]

$MAPbBr_3$ and $MAPbI_3$ are appropriate for tandem devices as well as for single-band gap absorbers, while $MAPbCl_3$ is more beneficial for light-emitting applications.[67] Though, for the perovskite devices the halide mixing offers extra benefits in terms of stability, band gap adjustment, and improved carrier transport. Lee *et al.* reported that the blend of halide perovskite $MAPb(I_{1-x}Cl_x)_3$ offers stability benefits over $MAPbI_3$ while synthesizing in the air.[68] Noh *et al.* established that mingling 20–29% Br into $MAPbI_3$ meaningfully improved the stability of the perovskite devices while sustaining the cell's performance.[69]

Additionally, greater electron–hole diffusion lengths were observed for $MAPb(I_{1-x}Cl_x)_3$ compared to $MAPbI_3$, whereas the $MAPb(I_{1-x}Br_x)_3$ and $MAPb(Br_{1-x}Cl_x)_3$ showed fewer rates of carrier recombination and improved carrier movement.[70–82] Though, it is difficult to produce mixed (I, Cl) perovskite less than 625 K, whereas it is easy to synthesize mixed (Br, Cl) and (I, Br) perovskites at room temperature.[83–90] Jeon *et al.* showed that $(FAPbI_3)_{0.85}$ $(MAPbBr_3)_{0.15}$ has numerous benefits compared to blends such as $FAPbI_3$, $MAPbI_3$, and $MAPb(I_{0.85}Br_{0.15})_3$.[58] Jacobsson *et al.* exhibited that a minor change in the chemical structure will have a prominent effect on the perovskite materials characteristics and eventually enhance the cell performance in case of a double-cation double halide mixed PSCs.[71,91–98] Moreover, as discussed already in the previous segments, scholars are combining more cations (triple, quadruple) with the mixed halide to obtain enhanced stability and performance.[61,99–112]

## 3. Electron-transporting materials

ETL, is occasionally called an electron collection or extraction layer, where electrons are inserted from the perovskite absorber

Open Access Article. Published on 02 1402. Downloaded on 14/11/1404 12:16:38 ..
This article is licensed under a Creative Commons Attribution-NonCommercial 3.0 Unported Licence.

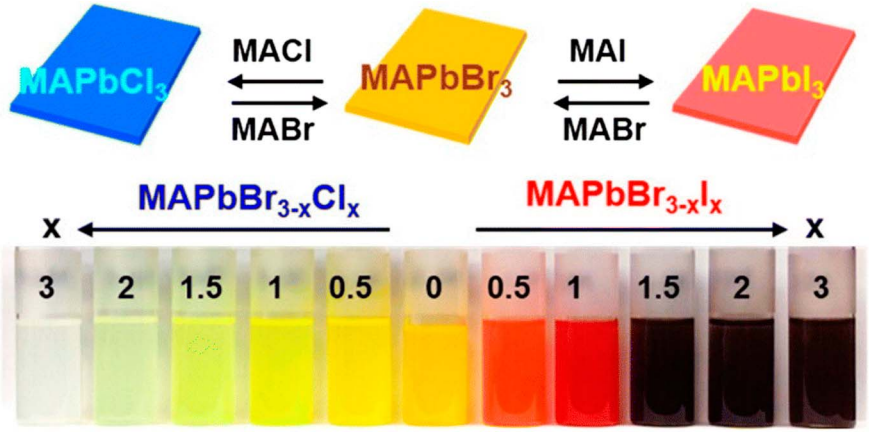


Fig. 9 Snapshots of halide replacement/mixing in the perovskite assembly (reproduced with permission from ref. 66, copyright 2014 ACS).

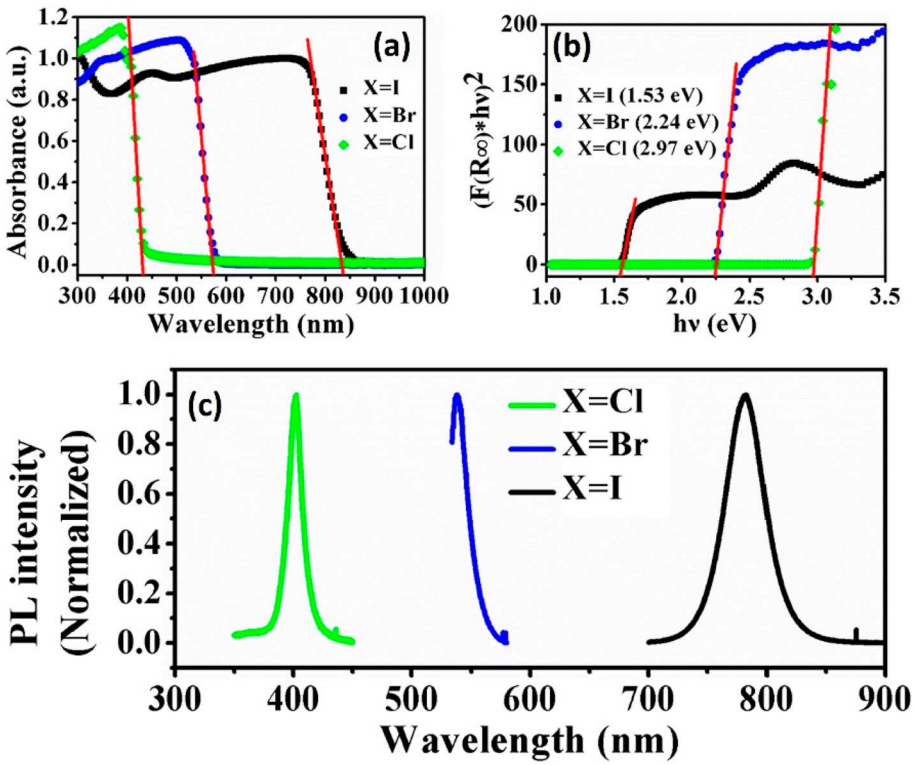


Fig. 10 Influence of halide replacement on the optoelectronic characteristics of perovskites: (a) absorption spectrum, (b) band gap, and (c) photoluminescence spectrum (reproduced with permission from ref. 70, copyright 2014 Elsevier).

layer, moved over the electron transporting materials (ETM), and lastly together with the metal electrode. ETL can be substituted with a fused photoelectrode to enhance the charge-gathering productivity by dropping the series resistance.[113,114] Furthermore, ETLs composed of one-dimensional nano-structures can provide rapid charge transport in solar cells.

A schematic illustration of PSC architecture is shown in Fig. 11. The universal arrangement of PSCs classically comprises a light-absorbing layer that is reversed between ETL, along with FTO, and metal electrodes are assisted as a glass substrate and back electrode, separately.[115–117] The detailed working and charge transport mechanisms are defined in Fig. 11a–c. The hole and electron shadowing in the device construction causes a more recombination rate. In a planar heterojunction PSC, the performance can be prominently enhanced by creating suitable pathways for both holes and electrons.[118,119.]

ETLs are films having a conduction band minimum (CBM) that must be inferior to that of a perovskite light absorber.[120–122] The perovskite devices investigations initiated with $TiO_2$ as an

 © 2023 The Author(s). Published by the Royal Society of Chemistry

Open Access Article. Published on 02 1402. Downloaded on 14/11/1404 12:16:38 ..
This article is licensed under a Creative Commons Attribution-NonCommercial 3.0 Unported Licence.

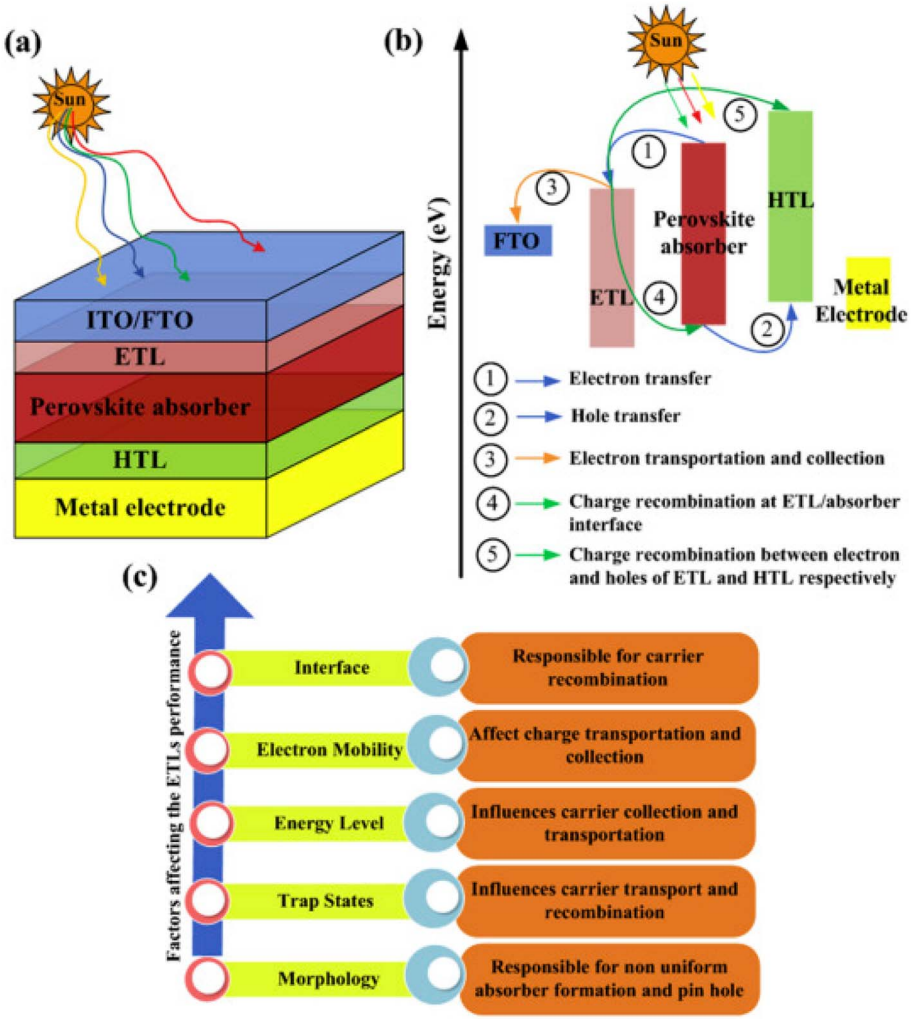


Fig. 11 (a) PSC assembly. (b) Graphic depiction of working and charge transference routes in ETLs of PSCs. (c) Factors influencing the ETL efficiency in PSCs (reproduced with permission from ref. 114. Copyright 2022 Elsevier).

ETL back in 2009, when a solar device was considered using a Pt-covered FTO as a glass substrate and $CH_3NH_3PbBr_3$ as a light absorber, respectively.[12] Exploration in PSCs explicitly emphasizes low-temperature layers deposition, which introduces various better other ETLs, such as CdS, $In_2O_3$, $Fe_2O_3$, $In_2S_3$, $Nb_2O_5$, $Zn_2SO_4$, and IGZO have also been extensively used in PSCs.[123–125] Indeed, organic ETLs have also revealed their occurrence in PSCs with lesser recombination rates and hysteresis.[126,127] Additionally, diverse approaches such as multilayer research of ETL, thickness variation and alteration in dopant concentration, and growth of novel nanostructures, along with surface and interfacial engineering methods were approved for highly stable and high-performance PSCs.[128,129] In order to select a proper ETL, the following things should be considered. The material should avoid the chemical reaction with adjacent light-absorbing material and electrodes. Better and dense morphology of the films is needed to restrict the drip from the films and pinhole. The widely used ETLs in PSCs are $TiO_2$, $SnO_2$, and CdS.[130–132]

### 3.1 Inorganic electron transporting layers

**3.1.1 Titanium oxide ($TiO_2$).** Since the last decade, titanium oxide has been recognized as a basic ETL in PSCs, owing to its low-temperature processing, better stability, and suitable optoelectronic characteristics.[133] The electronic properties of $TiO_2$ can be tuned easily by doping with Sn Ru, Li, Zn, Cd, Nb, and Zn cations. In a mesostructured cell, the ETL and perovskite absorber are accountable for electron transport and collection.[134–136] But, in planar structure PSC a better contact between the ETL/absorber is accountable for the transport of electrons. The very first PSC was introduced by Akihiro *et al.* having $TiO_2$ semiconductor producing PCE of 3.81%.[135,137] Wang *et al.* used anatase and rutile phase $TiO_2$ and revealed that rutile phase $TiO_2$ is more helpful in the collection and transport of electrons.[138] Additionally, organized $TiO_2$ nanocones using the simplest hydrothermal method were synthesized by Zhong *et al.* As revealed in Fig. 12a–d, the development of $TiO_2$ nanocones is a function of growth time.[139]

Many studies also showed that the device efficiency can be enhanced after doping metal cations in $TiO_2$ ETL, which

Open Access Article. Published on 02 1402. Downloaded on 14/11/1404 12:16:38 ..
This article is licensed under a Creative Commons Attribution-NonCommercial 3.0 Unported Licence.

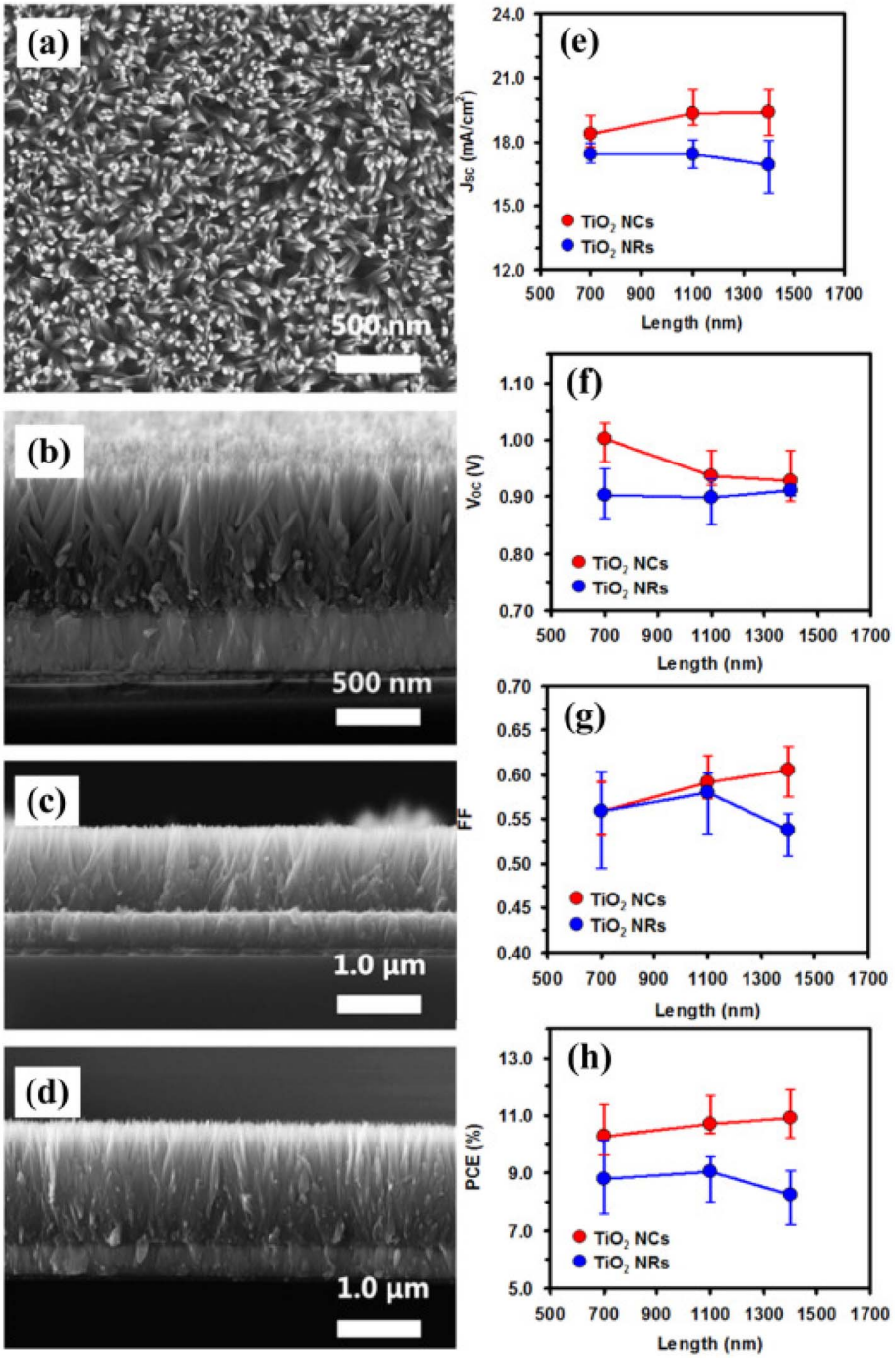


Fig. 12 (a) Top view of nanocones and (b) side view of SEM image of $TiO_2$ nanocones grown over FTO glass substrate (a and b) with 700 nm, (c) 1100 nm, (d) 1400 nm, $TiO_2$ nanocones. Comparative works of both $TiO_2$ nanocones and nanorods for 16 devices having various physical parameters (e) $J_{SC}$, (f) $V_{OC}$, (g) FF, and (h) PCE of PSCs with respect to length (reproduced with permission from ref. 139. Copyright 2015 Elsevier).

improves the charge collection and light-capturing ability.[136] To decrease the carrier buildup at boundaries and improve the charge transport in current years 2D materials and graphene have been also explored. The architecture is fabricated of four devices with the following ETLs.[140]

- graphene mesostructured $TiO_2$ (ETL1) + mesostructured $TiO_2$ (ETL2)
- mesostructured $TiO_2$ + graphene oxide (GO) having Li interlayer (ETL3)
- graphene + mesostructured $TiO_2$ + GO as Li interlayer (ETL4)

For the ETL4 sample, the crystalline quality is much superior compared to other ETLs.

**3.1.2 Zinc oxide (ZnO).** ZnO is another ETL having better optoelectronic characteristics and a CBM of 4.2 eV of CBM. It was


© 2023 The Author(s). Published by the Royal Society of Chemistry

Open Access Article. Published on 02 1402. Downloaded on 14/11/1404 12:16:38 ..
This article is licensed under a Creative Commons Attribution-NonCommercial 3.0 Unported Licence.

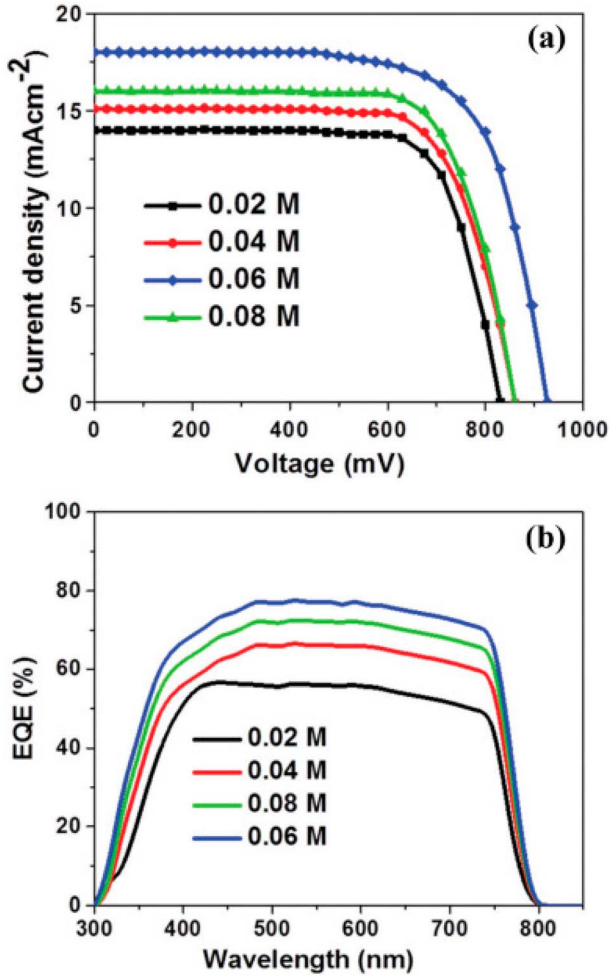


Fig. 13 (a) *J–V*, and (b) EQE properties of PSCs as a function of precursor concentration 0.02 M, 0.04 M, 0.08 M, 0.06 M (reproduced with permission from ref. 145. Copyright 2014 RSC).

applied as a hexagonal wurtzite structure in PSCs. There are some properties that make it appropriate for flexible devices owing to film processing at low temperatures and high conductivity.[141–144] Firstly, Liu and Kelly attained a PCE of 15.7% in PSC with ZnO as ETL.[143] It was revealed that a mesoporous scaffold structure and high-temperature processing are not permanently compulsory to achieve high PCE in PSCs.

The enhancement in electron gathering and transport can be attained by:

- interaction between the ETL and light-gathering film should be proper
- choice of TCO
- metal cations should be tailoring ETLs
- By introducing nanostructured electron transfer material

Furthermore, to improve the performance and reduce the recombination losses Mahmood *et al.* introduced a concept of double-layer ZnO nano-structured.[145] The hydrothermal method by which a double-layer ZnO nanostructure is formed causes the growth of nanorods on ZnO sheets. The density of ZnO nanorods was controlled by varying ZnO solution concentration from 0.02 M to 0.06 M. For 0.02 M to 0.06 M *J–V* curve and EQE spectra are revealed in Fig. 13a and b. As the concentration increased to 0.06 M, the $J_{SC}$ value increased. Similarly, the PCE enhanced from 6.98% to 10.35% and $V_{OC}$ improved from 0.83 V to 0.928 V.

Wang *et al.* using indium zinc oxide (IZO) as ETL achieved a PCE of 16.25% with insignificant hysteresis.[146] Cao *et al.* fabricated the hysteresis-less and constant PSC by depositing a thin film of MgO over the ZnO surface (Fig. 14).[147]

The interfacial approach was adopted to improve the stability and photovoltaic characteristics of PSCs.

**3.1.3 Tin oxide ($SnO_2$).** An alternative familiar inorganic ETL is becoming a relatively ideal $SnO_2$ because of its deeper conduction band and wider bandgap from 3.6 eV to 4.1 eV. Because of several advantages, $SnO_2$ has been deemed the utmost talented candidate in PSCs as ETLs. Dong *et al.* using the sol–gel method prepared a nanocrystalline $SnO_2$ and employed it as an ETL.[149] Li *et al.* fused a mesoporous film of $SnO_2$ as ETL in perovskite devices in place of conventional $TiO_2$.[148,149] They changed the $SnO_2$ film breadth to assess the device efficiency. With the increased thickness the IPCE also improved along with PCE.

To date, the main concern for PSCs is long-term stability. This aspect was not explained much for $SnO_2$ ETL-based PSC devices. Choi *et al.* for the construction of thermally steady PSCs, fused 3-(1-pyridinio)-1-propanesulfonate zwitterionic composite in $SnO_2$ ETL. The zwitterions compound has some advantages[150]

- It enhances the transportation ability to ETL from the perovskite absorber and also the electron collection ability
- Back transport of electrons from the collection film to the perovskite light absorber prevents the formation of an interfacial dipole
- Charge extraction improvement and enhancement of built-in potential is by the incorporation of zwitterion
- The positively charged atoms of zwitterion enrich the device's stability

Yoo *et al.* for managing the charge transport in PSCs reported an innovative approach. Initially, they established $SnO_2$ as ETL.[151] Then, between the interfaces, and bulk passivation method was implemented that enhanced the film quality. They divided the growth variation into stage B and stage A. Stage A is further divided into three parts A-i having pH 1 with acidic nature, A-ii having pH 1.5, and stage A-iii having pH 3. Stage B showed the ultimate response with diverse morphology at extreme pH 6, Fig. 15 represents the growth device with the presentation of various stages.

### 3.2. Organic ETLs

**3.2.1 Fullerene ($C_{60}$ and $C_{70}$).** In the case of organic ETL typically in the case of inverted PSCs, fullerene has received significant attention. Through the vacuum deposition technique and low-temperature processing technique, the material can reduce the hysteresis. Solution-based fullerenes have an excellent passivation technique that eventually reduces the trap state density.[152,153] To enhance the device performance, Ke *et al.* studied the vacuum processing of a dense $C_{60}$ ETL. Because of

Open Access Article. Published on 02 1402. Downloaded on 14/11/1404 12:16:38 ..
This article is licensed under a Creative Commons Attribution-NonCommercial 3.0 Unported Licence.

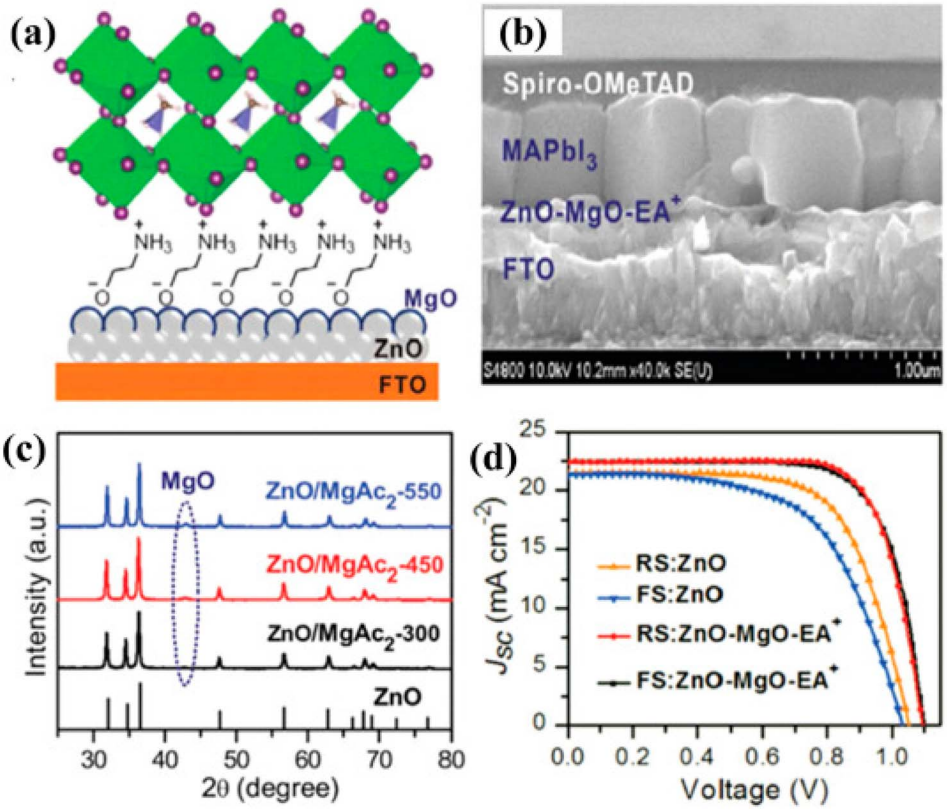


Fig. 14 (a) Graphic depiction of altered planar perovskite thin-film assembly with ZnO-MgO-EA$^+$. (b) SEM image exhibiting the side view of the device. (c) XRD arrangement of the precursor solution having diverse temperature environments. (d) $J_{SC}$–$V$ curves. (Reproduced with permission from ref. 147, Copyright 2018 Wiley-VCH).

less compatibility with solvents, the growth of the compact $C_{60}$ faced severe problems. So, mostly the compact-$C_{60}$ was formed *via* the thermal evaporation method that presented a flat surface.[152]

Intense care is needed for the processing of layer development at low-temperature especially in PSCs. Yoon *et al.* produced vacuum-formed $C_{60}$ electron selective film, treated at room temperature. Variation in device performance was observed as a function of bathocuproine (BCP) addition. The devices with BCP interlayer showed enhanced output due to the significant electron extraction characteristics. Hysteresis-less devices were also fabricated by using $C_{60}$ ETL on polyethylene naphthalate (PEN) substrates showing high device performance.[153]

The developed device under 1-sun illumination showed a PCE of 18.2% with a small hysteresis current. The commercialization of these ETLs hindered due to the higher cost of the fullerenes derivative. Xu *et al.* studied the mixture of $C_{60}$ and $C_{70}$ as the pristine fullerene mixture (FM). The solubility was improved due to enhanced configurational entropy up to 52.9 g $L^{-1}$, which through the spin-coating technique showed a reduction in the crystallization rate of FM.[154] The PEC of the developed device with FM ETL was 16.9%. Pascual *et al.* deposited a $C_{70}$ layer on an FTO glass substrate. The device delivered a PCE of 13.6% made-up of cell arrangement of FTO/$MAPbI_3$:$C_{70}$/Spiro-OMeTAD/Au.[155]

**3.2.2 Fullerene derivative.** In inverted PSCs, the phenyl-$C_{61}$-butyric acid methyl ester (PCBM) usually used as a fullerene derivative owing to greater solubility with the capability to decrease density traps and high electron transportation properties. $C_{70}$ and $C_{60}$ are less expensive.[156,157] In PSCs, researchers have also reported organic ETLs along with inorganic ETLs. Guo *et al.* deposited silver nanowires (Ag NWs) using a solution-based technique to investigate the performance of transparent PSCs. The device showed a PCE of 8.49% with $V_{OC}$ of 0.96 V, FF of 66.8%, and $J_{SC}$ of 13.18 mA cm$^{-2}$ made up with an arrangement of ITO/PEDOT:PSS/absorber/$PC_{60}$BM/ZnO/AgNWs.[158] A diagram of the prepared device is revealed in Fig. 16a and b illustrating the phase separation. Fig. 16c and d represents the cross-section image of the cell and energy level illustration.

PSCs having decent transparency has also gained much attraction. Keeping this in mind, Li *et al.* fabricated a PSC *via* a low-temperature-based film formation technique with PCBM ETLs.[161] The PSCs construction using classical PCBM is revealed in Fig. 17a–c displays the device construction explaining the absorber grain boundaries and the development of PCBM dispersed inside the ETL film. Top view of SEM and cross-sectional TEM image Fig. 19d and e show the development of PCBM-fused PSCs. Afterward, it was melted in


© 2023 The Author(s). Published by the Royal Society of Chemistry

Open Access Article. Published on 02 1402. Downloaded on 14/11/1404 12:16:38 ..
This article is licensed under a Creative Commons Attribution-NonCommercial 3.0 Unported Licence.

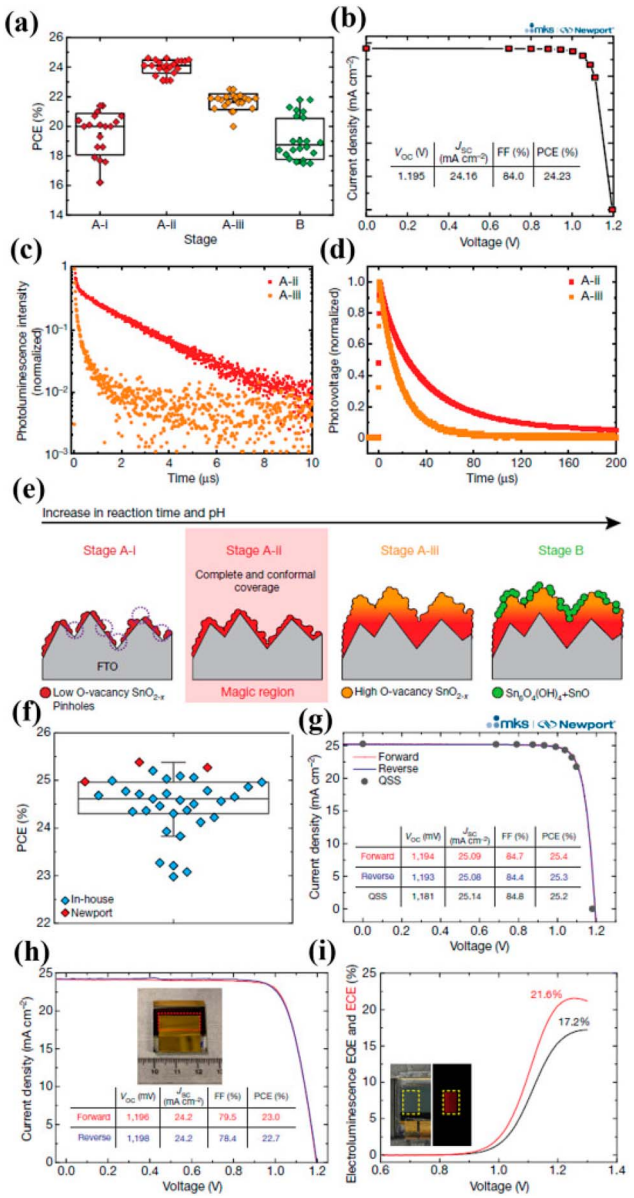


Fig. 15 (a) The difference in PCE of PSCs together with alteration in $SnO_2$ preparation phases. (b) Quasi-steady-state current density *vs.* voltage characteristic for stages A-ii. (c) Time-resolved photoluminescence study for perovskite absorber set for the stage A-ii (red trace), stage A-iii (orange trace) of $SnO_2$ ETL. (d) Transient photovoltage study for stage A-ii and stage A-iii, $SnO_2$-based PSCs. (e) The development stage of $SnO_2$ ETL. (f) Statistical spreading depiction in box-and-whisker plots for established PSCs. (g) *J*–*V* curves of the produced PSCs obtained at Newport. (h) *J*–*V* curve displaying supreme PCE of 23% under the active area of 0.984 $cm^2$. (i) Electroluminescence EQE and ECE findings of PSC under forwarding bias (reproduced with permission from ref. 151. Copyright 2021 NPG).

chlorobenzene the evolution of PCBM-supported ETL, produced an even and pinhole-free surface.

**3.2.3 Non-fullerene acceptors.** The modification of organic ETLs through doping is a really challenging task.[162] For the first time, Zhang *et al.* testified amino-substituted perylenediimide imitative to substitute the conservative $TiO_2$. Under the circumstances of low temperature and solution-based conditions, they have formed ETL both onto the FTO glass substrate and PET flexible substrate.[163] From the atomic force microscopy (AFM) results as revealed in Fig. 18a and c it originated that a tiny decrease in the irregularity of the perovskite absorber layer was observed, while the roughness of the PDI layer decreased to 3.59 nm from 13.0 5 nm. The *J*–*V* plots are displayed in Fig. 18d–f, along with the PDI molecular structure. One more n-type organic electron-accepting material in PSCs is naphthalene diimide (NDI). As a good electron-selecting material for PSCs, the NDI support and phosphite were imposed.

The development of ETM is vital for refining the performance of PSCs. Both inorganic and organic material-based ETMs can be utilized in PSCs; characteristically, inorganic ETLs are widely used in conventional cell construction while organic materials are utilized in inverted devices.[165] The energy stages of the most commonly used inorganic and organic ETLs utilized in PSCs are shown in Fig. 19 and 20, respectively.[166]

Currently, owing to prominent electron-transport characteristics, $TiO_2$ is the widely used ETL in the classical n–i–p PSC construction.[167] However, the high sintering temperature is needed to attain the desired crystallinity, which makes it unsuitable to use in PSCs in order to achieve high performance.[168–173] Therefore, the need for a low-temperature method for the fabrication of $TiO_2$ film is dynamic these days. Coning *et al.* established a sol–gel procedure to prepare $TiO_2$ nanoparticulate ETL and obtain a PCE of 13.6%.[169] Yella *et al.* also recognized a low-temperature production method employing nanocrystalline rutile $TiO_2$ formed using a chemical bath deposition technique, and they achieved a PCE of 13.7%.[174] Wu *et al.* established the utilization of low-temperature (<100 °C) solution-based $TiO_x$ ETL in PSCs and achieved a high PCE of 17.6%.[172] In the case of UV light, it has been initiated that $TiO_2$ ETL-based devices have low stability, which could be a test towards the industrialization of $TiO_2$-based PSCs.

Jiang *et al.* introduced a clear luminescent down-converting film of Eu-complex (Eu-4,7-diphenyl-1, 10-phenanthroline) to improve the light employment and initiate that integrating an Eu-complex film aided to improve 11.8% $J_{SC}$ and 15.3% PCE caused by re-emitting UV light (300–380 nm) in the visible region unlike the uncovered any down alteration film.[175,176] Furthermore, the electron injection amount from the photoactive perovskite absorber film to the $TiO_2$ ETL is very rapid, this is balanced rather by high electron recombination rates due to low electron movement.[177] Therefore, there is much attention on discovering other inorganic ETLs to improve the stability and performance of PSCs.[178] As compared to $TiO_2$, ZnO possesses much electron movement and can be simply deposited using a low-temperature method without sintering[179–181] Researchers have also reported ZnO ETLs, which efficiently improve the charge collection productivity and performance of perovskite devices.[231–234] In recent times, $SnO_2$ has been assessed as an alternative and superior ETL owing to its exceptional properties such as high optical transmittance, high electron movement, and varied band gap. Li *et al.* effectively

Open Access Article. Published on 02 1402. Downloaded on 14/11/1404 12:16:38 ..
This article is licensed under a Creative Commons Attribution-NonCommercial 3.0 Unported Licence.

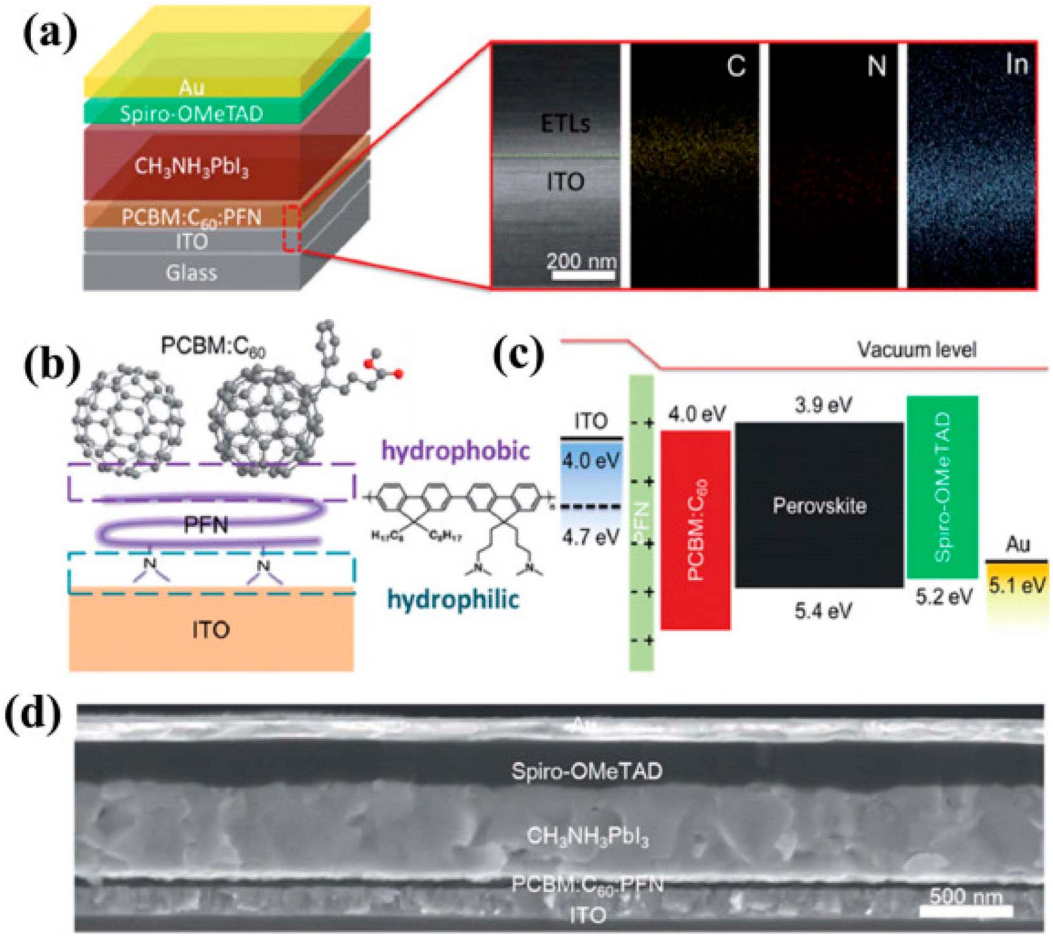


Fig. 16 (a) Illustrative depiction of the produced thin-film assembly and SEM image with EDS plotting of the cross-section of ITO/PCBM:$C_{60}$:PFN (approx 120 nm). (b) Symbolic drawing of vertical phase parting in the ternary PCBM:$C_{60}$:PFN and molecular structure of PFN. (c) Energy figure, and (d) SEM image showing the side view of the established device (reproduced with permission from ref. 159. Copyright 2018 RSC).

introduced $SnO_2$ ETL and they accomplished PCE above 10%.[182] Mohamadkhani *et al.* established that by means of low-temperature-method $SnO_2$ ETL in a straightforward planar PSC construction could produce PCEs of as high as 13.0%, with extraordinary stability.[183] although $SnO_2$ possesses outstanding electrical and optical properties and can be synthesized using a low-temperature solution-processed method, the prominent hysteresis detected in the cells using $SnO_2$ ETL is interrupted for these PSCs. In order to reduce this issue, Baena *et al.* fabricated a 15 nm-thick $SnO_2$ electron-selective layer (ESL) using a low-temperature atomic layer deposition (ALD) method and attained a barrier-less band configuration between the mixed perovskite ($(FAPbI_3)_{0.85}(MAPbI_3)_{0.15}$) material and $SnO_2$ and thus producing a effective/hysteresis-less planar PSCs (Fig. 21).[184] By combining the film deposition techniques such as spin-coating (Fig. 22a) and chemical bath deposition (Fig. 22b), the bumpiness and consistency of the ETL were enhanced, and subsequently, the blocking abilities of the $SnO_2$ film were enhanced (Fig. 22e).[185]

Indium oxide ($In_2O_3$) is also an alternative talented ETL that shows outstanding electrical and optical and electrical characteristics, namely better light transmission, fast electron movement, and wide band gap. Employing these benefits, Zhang *et al.* synthesized a solution-based $In_2O_3$ nanocrystalline film ETL for PSCs and attained a PCE above 13%.[186] Tungsten oxide ($WO_x$) is alternative, likely, latent n-type material for ETLs that has decent chemical steadiness, a wide band gap, and high electron movement. Chen *et al.* used $WO_x$ as an ESL in PSCs *via* a facile and solution-processed method, which showed equivalent light transmission and PCE to $TiO_2$, although, they gained an inferior $V_{OC}$.[187]

Owing to some outstanding properties such as better chemical and thermal stability and wide band gap, $CeO_x$ is also being employed as a talented material for ETLs. However, $CeO_x$ has already been utilized in diverse solar cells for its excellent properties, and Wang *et al.* stated used that $CeO_x$ as an ETL material for PSCs.[185–190] They established that $CeO_x$-based PSCs could be fabricated using a simplistic sol–gel technique at a low temperature (150 °C). $CeO_x$-based planar PSCs attained PCE of as high as 14.32% with decent stability.[191–196]


© 2023 The Author(s). Published by the Royal Society of Chemistry

Open Access Article. Published on 02 1402. Downloaded on 14/11/1404 12:16:38 ..
This article is licensed under a Creative Commons Attribution-NonCommercial 3.0 Unported Licence.

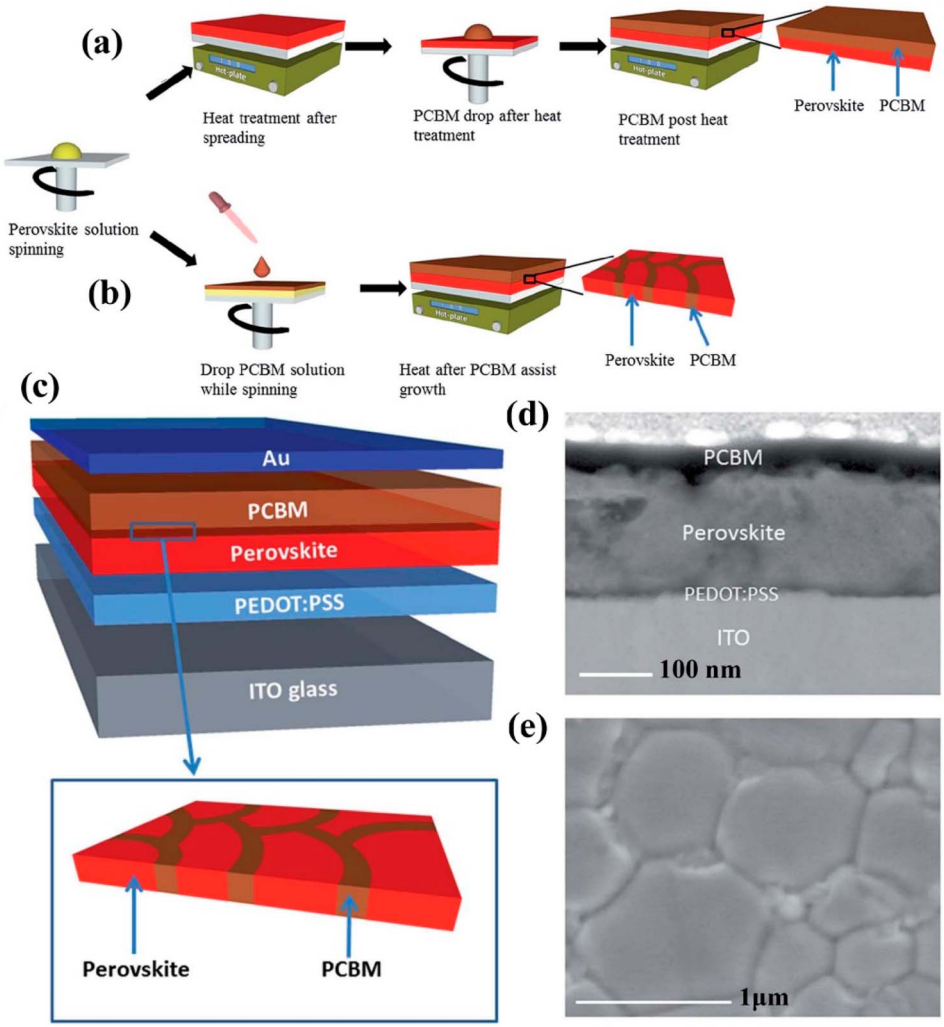


Fig. 17 Symbolic depiction of the development of PSCs, (a) using classic PCBM preparation route, (b) PCBM-supported preparation route. (c) Device construction of PSC using hybrid PCBM – absorber film, (d) cross-section TEM image of established PSC, and (e) top-view SEM figure of as-prepared perovskite absorber produced using chlorobenzene (CB)-supported method.[160] Three different PSCs comprising of single perovskite layer, perovskite/PCBM bilayer, and polymerized formula designed by Zhong *et al.* using temperature-based chronoamperometric examination and by dropping ionic motion the enhanced activation energy was noticed (reproduced with permission from ref. 161. Copyright 2020 Wiley-VCH).

## 4. High-efficiency PSCs fabrication approaches

### 4.1. Solution-based methods: one-step *versus* two-step coatings

In order to fabricate the perovskite absorber layer, usually two approaches are existed, namely, one-stage and two-stage coating approaches. In a one-stage method, a perovskite film was formed *via* spin-coating a blend of $PbI_2$ and $CH_3NH_3I$ solution (one-step layer formation) and by spin-coating $CH_3NH_3I$ later covered with $PbI_2$ (two-stage process). In the case of one-stage layer formation, $PbI_2$ and $CH_3NH_3I$ $CH_3NH_3I$ are completely melted using a suitable solvent such as dimethyl sulfoxide (DMSO), *N*,*N*-dimethylformamide (DMF), and gamma-butyrolactone (GBL) utilized as a layer formation solution. After spin-coating, drying, and annealing are performed. While, in a two-stage film formation process, a layer of $PbI_2$ was formed by dropping a solution of $PbI_2$ over the substrate surface and after that a solution of $CH_3NH_3I$ in 2-propanol was webbed over the $PbI_2$ layer (as exhibited in Fig. 23). Two-stage film formation approaches demonstrate better film morphology as compared to one-stage film formation method and resulted in a better cell efficiency,[197–199] which specifies that the control of perovskite absorber layer nanostructure is vital in attaining high-performance PSCs.

In a two-stage film formation approach, the dimensions of $CH_3NH_3PbI_3$ were pointedly reformed by the concentration of $CH_3NH_3I$.[200] As the concentration of the $CH_3NH_3I$ in a 2-propanol solution reduced from 0.063 M to 0.038 M, the typical $CH_3NH_3PbI_3$ crystal dimensions improved from about 90 nm to about 700 nm, as revealed in Fig. 24.

Open Access Article. Published on 02 1402. Downloaded on 14/11/1404 12:16:38 ..
This article is licensed under a Creative Commons Attribution-NonCommercial 3.0 Unported Licence.

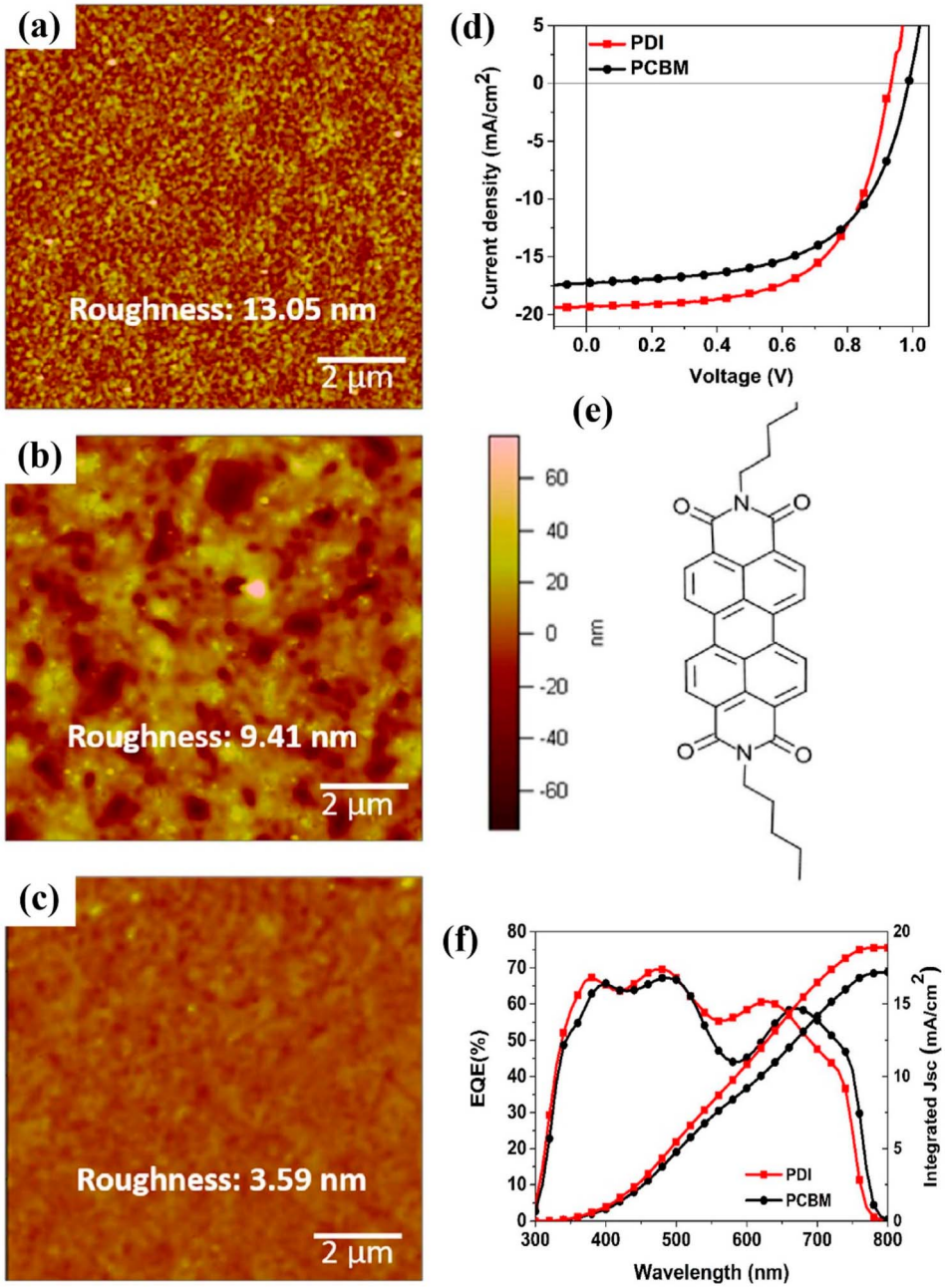


Fig. 18 AFM pictures of perovskite absorber ($CH_3NH_3PbI_{3-x}Br_x$) (a) prepared on PEDOT:PSS film, (b) after fabrication of PCBM, and (c) PDI film on PEDOT:PSS/perovskite thin layer. (d) *J*–*V* curves, (e) PDI molecular assembly, and (f) EQE-wavelength findings for both PCBM and PDI ETL-based PSCs (reproduced with permission from ref. 164. Copyright 2017 Elsevier).

Recently, a two-stage approach was comprehended *via* a blend of $PbI_2$ and $PbCl_2$. The solubility of $PbCl_2$ can be prominently improved using $PbI_2$ through common ion response. Wand *et al.* effectively melted $PbCl_2$ salt in DMF by adding $PbI_2$ and then deposited the blend over the mesoporous $TiO_2$ film.[201,202] After exposing it to the $CH_3NH_3I$ mixture, eventually a $CH_3NH_3PbI_{3-x}Cl_x$ perovskite film with precise morphology was fruitfully attained.[203] In Fig. 25, photovoltaic limits are shown as a function of $CH_3NH_3I$ concentration. For the 0.038 and 0.05 M samples, the average PCE was about 16.3%, while at much concentration of 0.063 M an inferior PCE of 13.4% was gained caused by lower FF and $J_{SC}$.

It was also observed that bulky crystals formed at lower solution concentrations resulted in superior $J_{SC}$ compared to smaller ones produced using the highly concentrated solution as can be seen in Fig. 25e, and an improved charge-drawing aptitude, as recorded by using photo-CELIV.[200,204] It can be clarified in conjunction with the photo-CELIV findings, that an alteration in $V_{OC}$ relates to the rates of charge-drawing and rumination.[201,205] In recent years, solvent manufacturing allowed better control over


© 2023 The Author(s). Published by the Royal Society of Chemistry

Open Access Article. Published on 02 1402. Downloaded on 14/11/1404 12:16:38 ..
This article is licensed under a Creative Commons Attribution-NonCommercial 3.0 Unported Licence.

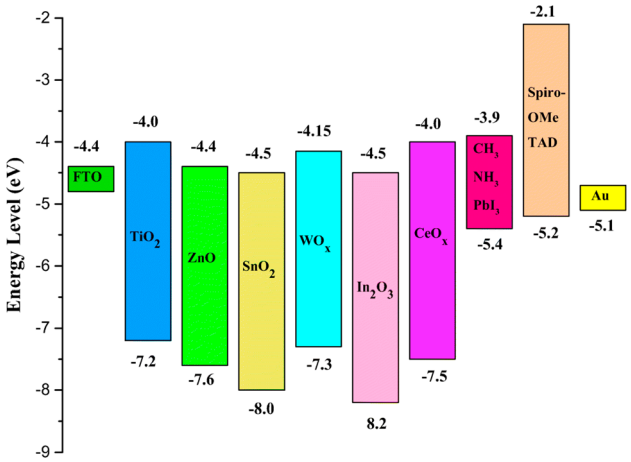


Fig. 19 Energy zones of diverse materials used as inorganic ETM in different films of PSCs (reproduced with permission from ref. 166. Copyright 2018 Springer).

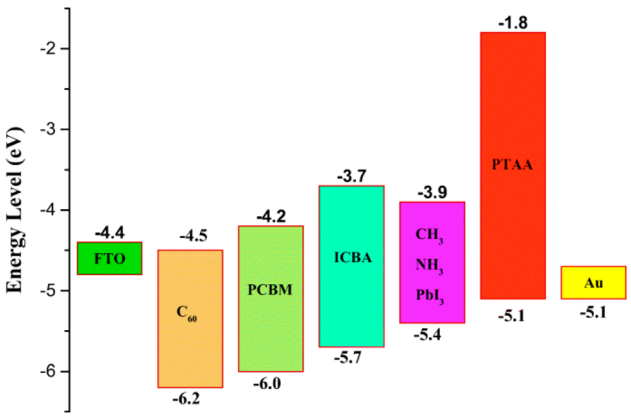


Fig. 20 Energy zones of diverse materials used as organic ETM in different films of PSCs (reproduced with permission from ref. 166. Copyright 2018 Springer).

the perovskite film morphology *via* solution-based methods, unlike vacuum approaches. Liu *et al.* described that a single-stage film formation approach was superior enough to fabricate even and smooth perovskite layers after it was exposed to chlorobenzene, which brought wild crystallization.[206–208] Seok's also introduced an ideal perovskite film formation method *via* the engineering of a solvent. They utilized a blend of solvents composed of dimethylsulphoxide (DMSO) and γ-butyrolactone trailed by toluene drop-covering, which resulted in the form of smooth perovskite film.[202,209,210] The droplet of toluene rapidly detached the extra DMSO solvent present in the wet layer, which directly satisfied the ingredients. To conclude, a regular smooth perovskite film was obtained after heating at 100 °C. Fig. 26 displays an X-ray diffraction (XRD) form of the middle and an SEM figure of the subsequent perovskite film displaying tightly-packed huge grains.

Additives such as $NH_4Cl$ influence the perovskite film was also considered. Ding and Zuo noted an 80.11% FF by adding an $NH_4Cl$ additive, which was initiated to improve the morphology and crystallinity of the perovskite film.[211]

### 4.2. Perovskite layer formation using the vacuum method

Perovskite layers can also be fabricated *via* the thermal decomposition of chemicals. Co-evaporation of $PbCl_2$ and $CH_3NH_3I$ results in a $CH_3NH_3PbI_3$ stage, and the film smoothness was much improved unlike the solution-based layers,[212] as shown in Fig. 27.

A two-source evaporation scheme with ceramic pots was fitted inside the nitrogen-filled glovebox. $PbCl_2$ and $CH_3NH_3I$ were co-evaporated using distinct containers with a molar ratio of 1 : 4. A dusky reddish-brown color was detected, instantly after the evaporation process. The crystallization of perovskite crystals was achieved by annealing.[212] Thermal evaporation needs an intense vacuum, which is an expensive way and limited the large-scale fabrication of devices. To overcome this issue, a vapor-supported solution method (VASP), which produces perovskite layers using onsite reactions of deposited layers of $PbI_2$ with $CH_3NH_3I$ vapor, was established.[213] The perovskite layer deposited with the help of this technique presented a better grain assembly with complete surface coverage.

### 4.3. Manipulation of perovskite absorber morphology

The morphology of perovskite has altered thoroughly since the development of new manufacturing ways and numerous mixed configurations. In this context, the prime task is the creation of high-performance perovskite layers with improved morphology, pinholes-free surface, and better surface coverage. The previous perovskite layers established a dot-like morphology using a one-step spin-coating method that twisted into a three-dimensional nanostructure after using a two-stage sequential deposition method. Furthermore, diverse knowledge has also been established, which is well-suited to the huge-area construction of the perovskite films to avoid the spin-coating method that was mostly utilized for lab-scale cells.

### 4.4. Effect of annealing environment perovskite absorber layer formation

The formation of the perovskite layer using a hot casting of a precursor solution over a heated surface requires extra handling with the heat of the perovskite layer, which is crucial. The circumstances of optimal annealing can also differ by changing the substrate type, layer thickness, and deposition method.[214–217] Dualeh *et al.* established the character of the annealing temperature on the formation of the perovskite layer.[215] The consequence of the diverse annealing temperatures was examined in the formation of perovskite films after spin-casting. Scanning electron microscopy (SEM) was used to study the effect of the annealing temperature on the perovskite layer (Fig. 28a–h). An extreme modification was detected in the morphology of the perovskite film at 80 °C (annealing temperature). When the annealing temperature was 100 °C, the perovskite layer was reasonably similar to that molded at 80 °C (Fig. 28b and c), in spite of the duration needed for the conversion was longer at 80 °C. Additionally, after the annealing temperature reached 120 °C, the

Open Access Article. Published on 02 1402. Downloaded on 14/11/1404 12:16:38 ..
This article is licensed under a Creative Commons Attribution-NonCommercial 3.0 Unported Licence.

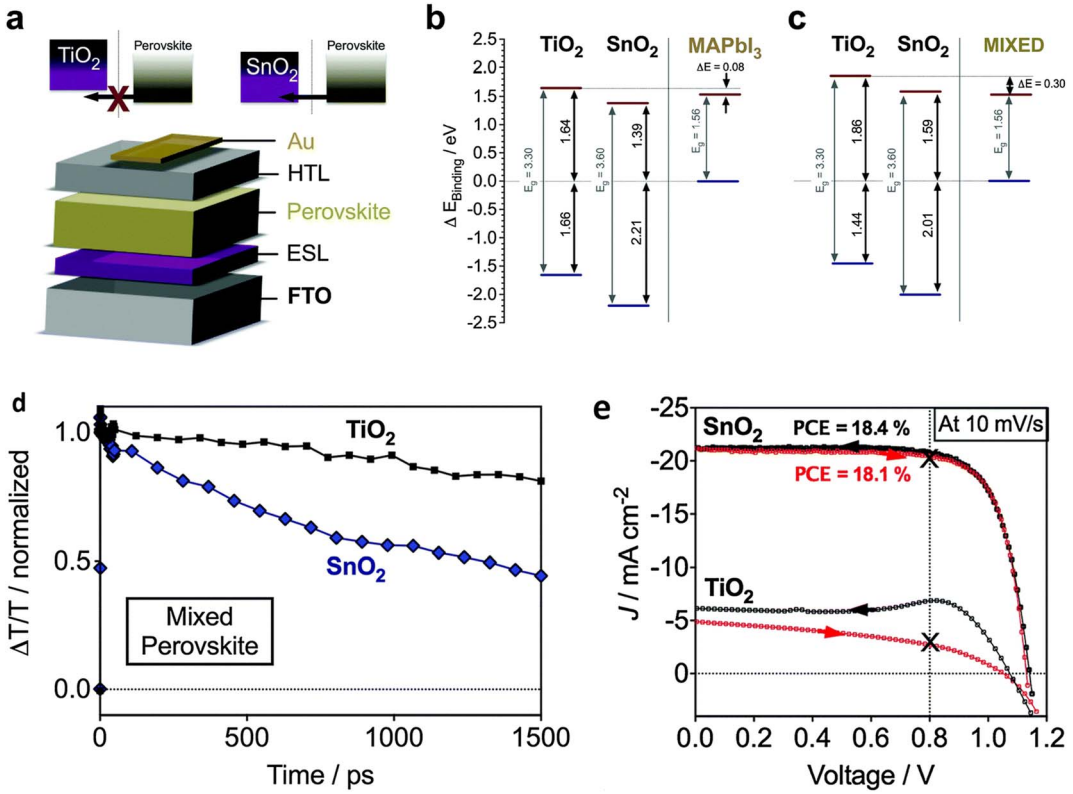


Fig. 21 (a–c). Diagram of energy level plans and electron inoculation properties of $SnO_2$- and $TiO_2$-based planar PSCs, (d) transient absorption findings, (e) current–voltage (*J–V*) curves of $TiO_2$- and $SnO_2$-based planar mixed halide-mixed cation PSCs (reproduced with permission from ref. 184. Copyright 2015 RSC).

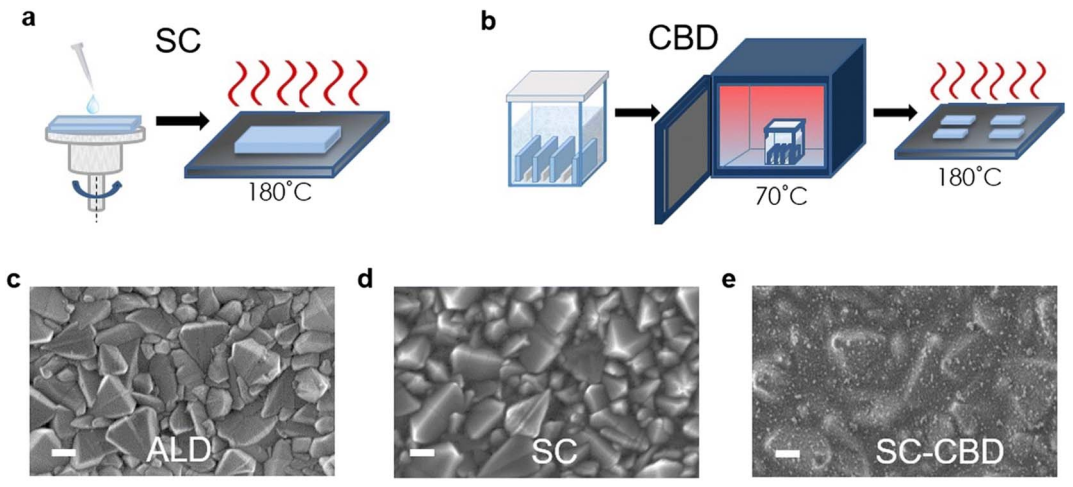


Fig. 22 Symbolic diagram showing the preparation of $SnO_2$ thin layers using (a) spin coating (SC) and (b) chemical bath deposition (CBD). (c) Top-view SEM pictures of $SnO_2$ films prepared by atomic layer deposition (ALD), (d) spin coating (SC), and (e) spin coating and chemical bath deposition (SC-CBD). All scale bars are 200 nm (reproduced with permission from ref. 74. Copyright 2016 RSC).

perovskite layer assumed a bigger separate size (Fig. 28d). It was detected that with the enrichment in the annealing temperature, perovskite crystals converted to a larger shape (Fig. 28e–g). Henceforth, Fig. 28a–g obviously proved that perovskite formation is meaningfully inclined towards annealing temperature. W. Nie *et al.* described a solution-processed hot-casting method to attain ~18% PCE with one millimeter-scale crystal grains.[218] It was noticed that grain size presented an exclusive leaf-like design glowing from the center of the grain (Fig. 28i). Though, Y. Deng *et al.* clarified a comparable type of design using Rayleigh–Benard convection, which springs a promising approach on millimeter-scale crystalline grains.[219]


© 2023 The Author(s). Published by the Royal Society of Chemistry

Open Access Article. Published on 02 1402. Downloaded on 14/11/1404 12:16:38 ..
This article is licensed under a Creative Commons Attribution-NonCommercial 3.0 Unported Licence.

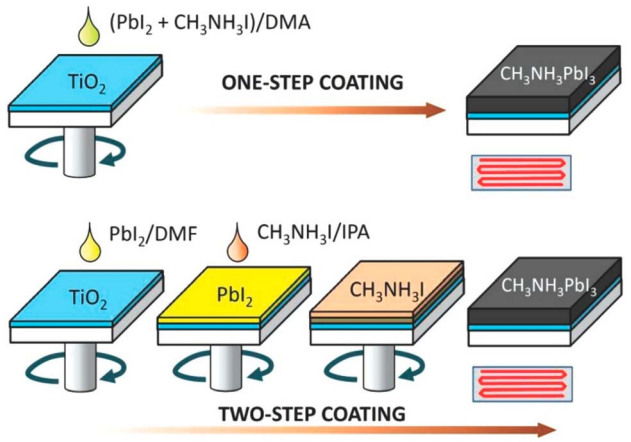


Fig. 23 One-stage and two-stage coating methods to prepare $CH_3NH_3PbI_3$ perovskite layers. DMA, DMF, and IPA signify dimethyl acetamide, dimethyl formamide, and isopropyl alcohol, respectively (reproduced with permission from ref. 197. Copyright 2014 AIP).

Muscarella *et al.* also established a novel, air-stable method for $CH_3NH_3PbI_3$ perovskites.[220] In Fig. 28l and m SEM micrographs of unannealed and annealed hot-deposited materials, respectively, are revealed, which discloses that the size of perovskite crystals rises throughout the post-formation annealing. Wu *et al.* stated the low-pressure supported method together with thermal heating in the film formation of double perovskite $Cs_2AgBiBr_6$.[221] Because of low-pressure dealing before annealing, double perovskite film presented dense and smooth morphology, unlike that in the conservative thermal annealing technique.

### 4.5. Formation of perovskite absorber layer as a function of precursor aging

It was detected that the aging of precursor has an prominent consequence on the formation of thin film, the density of the trap state, and uniformity.[222] P. Boonmongkolras *et al.* established the connection between the perovskite precursor solution aging period and the triple cation perovskite $Cs_{0.05}(FA_{0.83}MA_{0.17})_{0.95}Pb(I_{0.83}Br_{0.17})_3$ cell efficiency.[223] It was detected that cells that are made up using 6 hours old solution display the supreme average efficiency with the finest delivery and improved duplicability (Fig. 29a).

The deprivation structure in triple cation perovskite films was clarified by B. Dou *et al.*[224] The snaps of perovskite layers with loading days are revealed in Fig. 29b and the photographs of perovskite layers made-up from 24 days aged ink are exposed in Fig. 29c. It was detected that the perovskite film grows lighter with bigger storage days. The perovskite layer roughness and thickness were also influenced by solution aging.

### 4.6. Formation of perovskite absorber layer as a function of precursor temperature

PSCs are typically fabricated using preheated perovskite mixtures. G. Namkoong *et al.* discover the fundamental reason for the effect of temperature on PSCs. Perovskite ($MAPbI_{3-x}Cl_x$) solution was cast-off after heating using numerous temperatures of 40 °C, 70 °C, and 90 °C for 24 h, and thin layers were spin-coated in a nitrogen gas-filled glove box.[225] Fig. 30 displays the formation of $CH_3NH_3PbI_{3-x}Cl_x$ layers spin-casted over preheated glass substrate at 180 °C with dissimilar temperatures. The normal grain size at 70 °C is far greater compared to the solution heated at 40 °C, nevertheless, at 90 °C, there is a fall in grain size. The layer thickness was also affected by the solution temperature. Thickness was found as 210 ± 8 nm, 252 ± 7 nm, and 270 ± 6 nm using different solution temperatures of 40 °C, 70 °C, and 90 °C, respectively.

### 4.7. Effect of post-device ligand (PDL) treatment on the morphology of the perovskite absorber layer

H. Zhang *et al.* offered the elementary post-device ligand (PDL) behavior to meaningfully improve the stability and performance of PSCs.[225] In the report, diethylenetriamine (DETA) with three amine groups was used as a ligand to modify PSCs. In Fig. 31a and b top view SEM image is revealed and no big alteration in the grain size was detected after PDL treatment. The histograms of the cell efficiencies are shown in Fig. 31c.

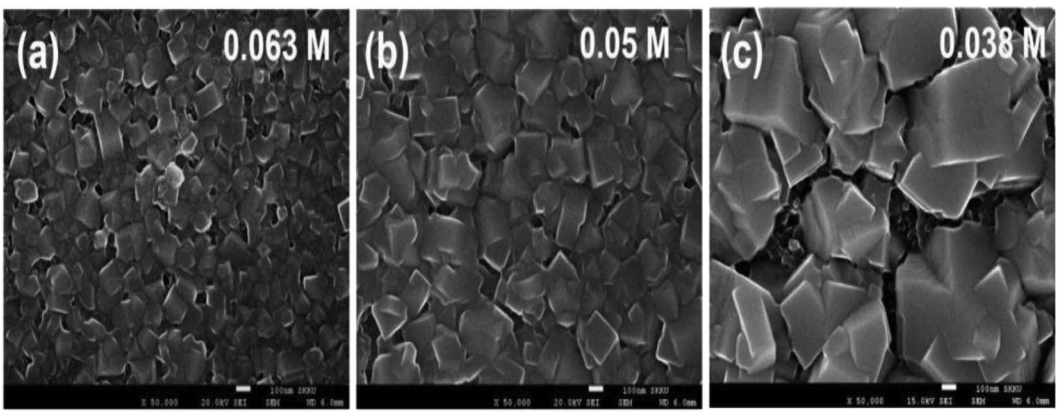


Fig. 24 SEM images for $CH_3NH_3PbI_3$ produced *via* two-step spin-coating with (a) 0.063 M, (b) 0.05 M, and (c) 0.038 M $CH_3NH_3I$ solution. Scale bars signify 100 nm (reproduced with permission from ref. 200. Copyright 2014 NPG).

Open Access Article. Published on 02 1402. Downloaded on 14/11/1404 12:16:38 ..
This article is licensed under a Creative Commons Attribution-NonCommercial 3.0 Unported Licence.

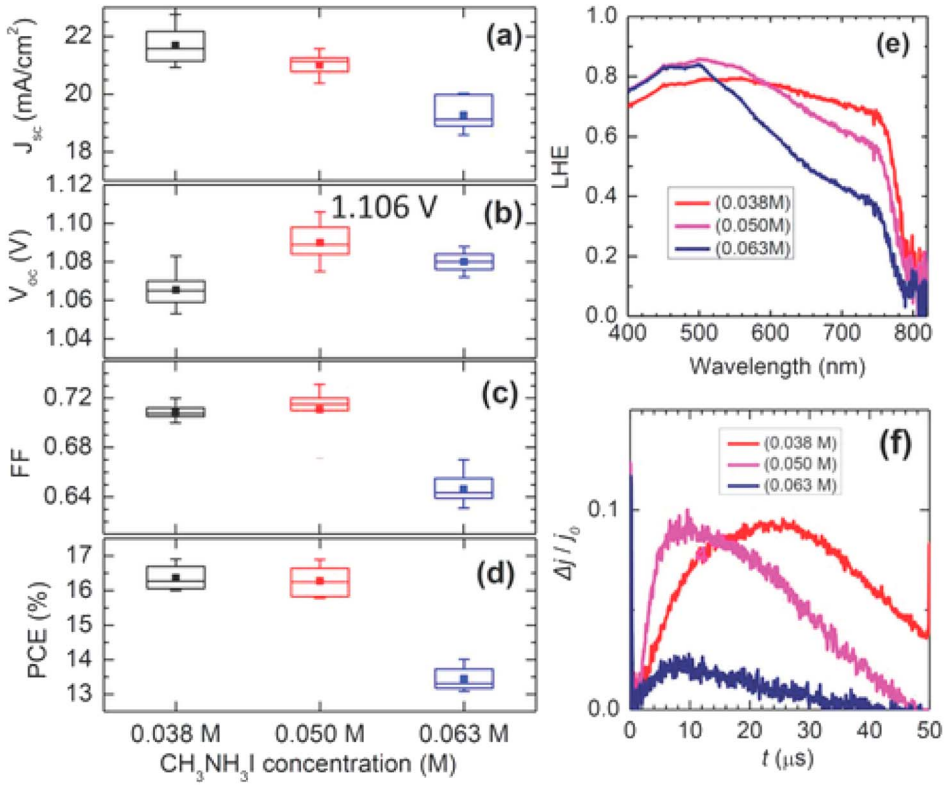


Fig. 25 (a–d). $J_{SC}$, $V_{OC}$, FF, and PCE, dependent on the $CH_3NH_3I$ concentration. Error bars in each box denote minimum and maximum values and the middle line in the box signifies the median value. Filled squares in the box denote mean values. (e) Light-capturing efficiency spectra of the $CH_3NH_3PbI_3$ layers laying on $CH_3NH_3I$ concentration. (f) Photo-CELIV transients noted for the cells containing FTO/bl-$Al_2O_3$/mp-$TiO_2$/$MAPbI_3$/Spiro-MeOTAD/Au, subject to $CH_3NH_3I$ concentration (reproduced with permission from ref. 200. Copyright 2014 NPG).

The PDL treatment significantly improves the device duplicability with a standard deviation of just 1.94%. In the short-term, the steadiness of the treated cells without any illustration astonishingly improves, with 70% efficiency reserved at ambient environments after a 500 hours maximum-power-point trailing trial, while the control device will totally break down within 100 hours.[225]

## 5. Role of interface engineering in perovskite devices

The development of interfaces in PSCs has been a real means to improve stability and photovoltaic performance. M. M. Tavakoli *et al.* established a perovskite device adopting an improved ETL with a PCE of 20.94% (Fig. 32a and b). A single layer of graphene was inserted at the boundary of ZnO ETL and perovskite light absorber. Amazingly, the author found that the insertion of a graphene monolayer at the ETL/perovskite border improves the carrier withdrawal and photovoltaic characteristics. Cell stability was further improved by passivating the perovskite layer using another modulator, *i.e.*, 3-(pentafluorophenyl)-propionamide (PFPA) to decrease the superficial trap states of the perovskite.[235] The stability findings display that the passivated device on MLG/ZnO retained 93% of its early PCE rate even after 300 h

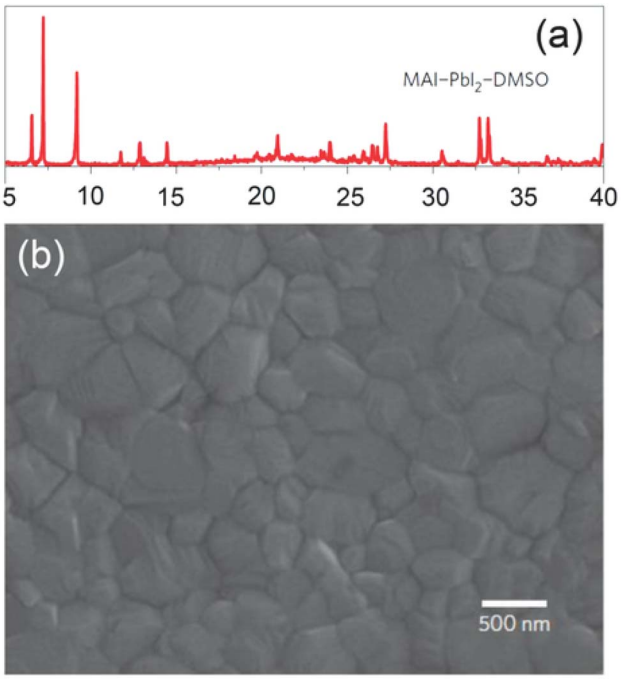


Fig. 26 (a) X-ray diffraction shape of an MAI-$PbI_2$-DMSO intermediate stage produced by toluene treatment on the layer deposited by spin-coating of MAI-$PbI_2$-DMSO-GBL solution. (b) SEM image of the subsequent perovskite layer using the middle stage (reproduced with permission from ref. 209 Copyright 2014 NPG).


© 2023 The Author(s). Published by the Royal Society of Chemistry

Open Access Article. Published on 02 1402. Downloaded on 14/11/1404 12:16:38 ..
This article is licensed under a Creative Commons Attribution-NonCommercial 3.0 Unported Licence.

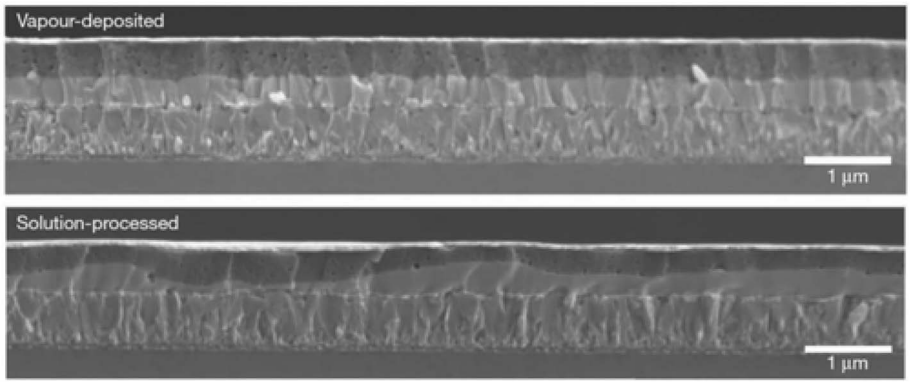


Fig. 27 Assessment of the perovskite layer consistency between vapor-deposition and solution-process approaches (reproduced with permission from ref. 212. Copyright 2013 NPG).

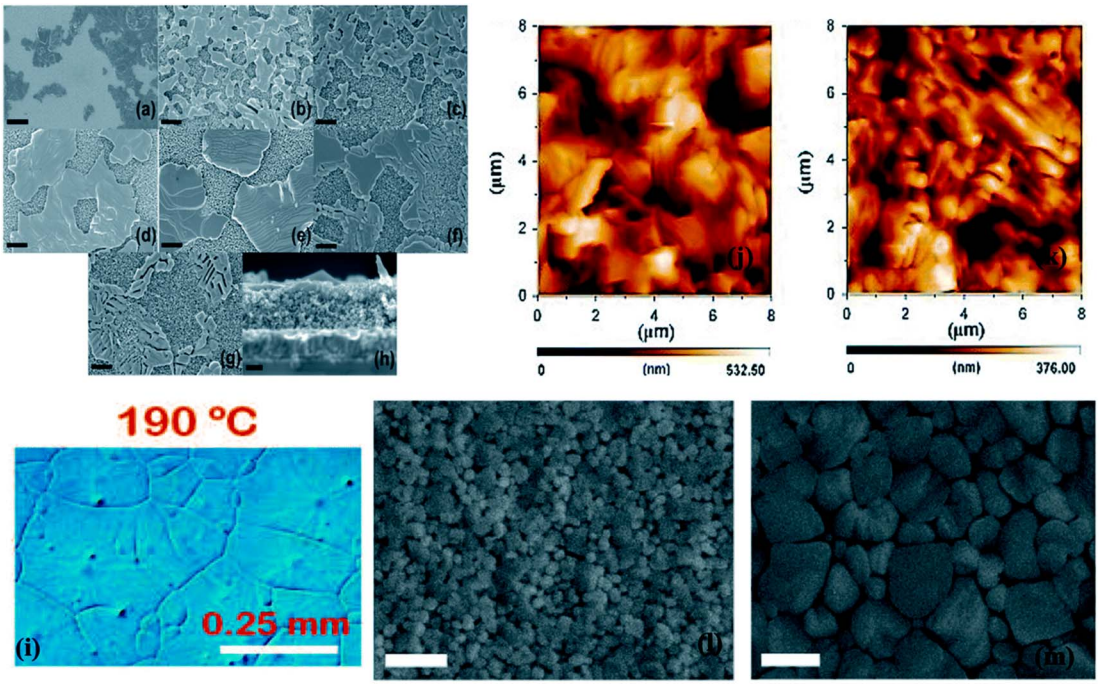


Fig. 28 Scanning electron microscope pictures of m-$TiO_2$ layers with the prepared perovskite solution heat-treated at various temperatures (a) 60 °C, (b) 80 °C, (c) 100 °C, (d) 120 °C, (e) 150 °C, (f) 175 °C, and (g) 200 °C. (h) Side view SEM image of the sample annealed at 150 °C. Black scale bars parallel to (a) 5 μm, (b–g) 1 μm, and (h) 200 nm[102] Optical micrographs of the $CH_3NH_3PbI_{3-x}Cl_x$ perovskite layer (i).[215] AFM pictures of perovskite layer toughened with the one-step technique (j), multi-step way (k) (reproduced with permission from ref. 218. Copyright 2015 AAAS). Scanning electron microscope picture of an unannealed hot-cast layer (l) and an annealed hot-cast layer (m), displaying that the perovskite crystals produce while annealing (reproduced with permission from [217] Copyright 2015 Elsevier).

under constant radiance (Fig. 32c). X. X. Gao *et al.* proved that by means of the conjugated polymers (PD-10-DTTE-7) with both the acceptor and donor alkylated as an interlayer between $MAPbI_3$ and doped Spiro-OMeTAD can meaningfully improve the efficiency of solar cells.[235]

Atomic-force microscopy (AFM) examination discloses that the roughness value was 24.6 nm for the $MAPbI_3$ layer and 16.3 nm for the PD-10-DTTE-7/$MAPbI_3$ film. Using the custom-made boundary, the $MAPbI_3$ devices with the PD-10-DTTE-7 interlayer displayed the best PCE of 18.83%. The surface nanostructure of dissimilar films was examined using a top-view SEM using various magnifications. Fig. 33a–c displays that tetracene and perovskite films are dense polycrystalline with micrometer grain size while Spiro accepts a conformal layer Fig. 33d, confirming total surface treatment of the mutual HTLs.[236] J. Lu *et al.* introduced a simple method to expand the PCE and elevated the PSCs stability by modifying the interface between the HTL and light-harvester.

Open Access Article. Published on 02 1402. Downloaded on 14/11/1404 12:16:38 ..
This article is licensed under a Creative Commons Attribution-NonCommercial 3.0 Unported Licence.

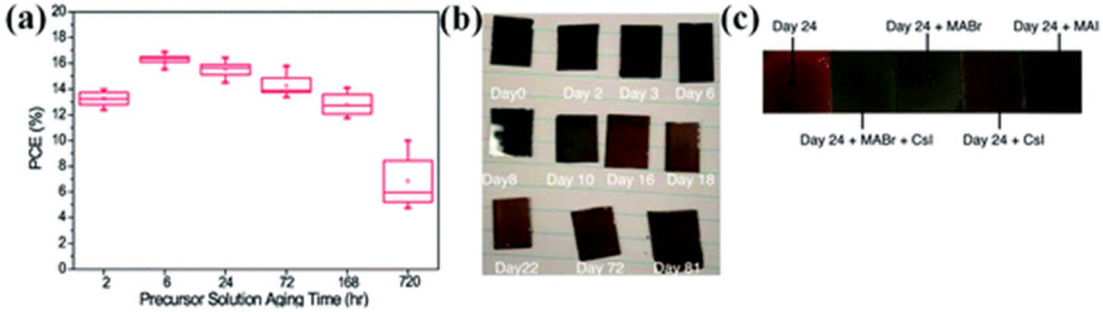


Fig. 29 (a) PCE distribution with precursor solution aging time (hours) of the triple-cation lead halide PSCs.[223] (b) Photographs of triple-cation (FA, MA, Cs) films produced from fresh ink (*viz.*, 0 days of storage, labeled as "Day 0") and the same ink is utilized for the 2–81 days storage. (c) Snapshots of layers made up from 24 days old ink. (Reproduced with permission from ref. 224. Copyright 2020 ACS).

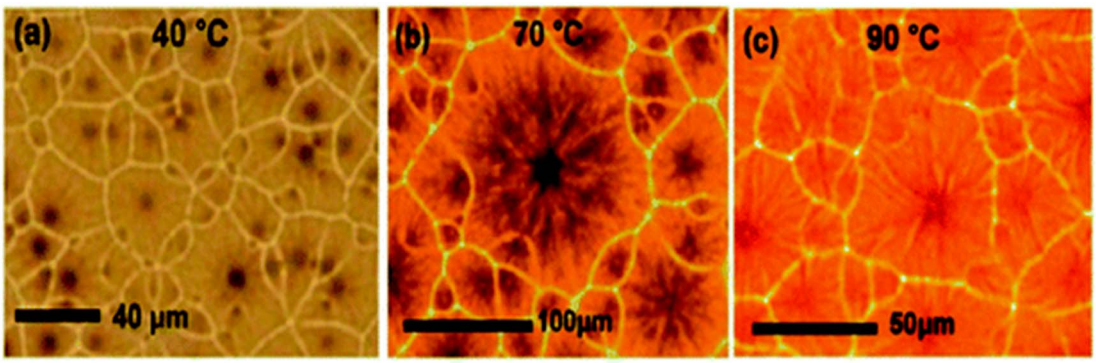


Fig. 30 Optical microscopic images of the perovskite thin layer by varying perovskite solution temperatures of (a) 40 °C, (b) 70 °C, and (c) 90 °C (reproduced with permission from ref. 225. Copyright 2018 Elsevier).

Using replicated solar cell working environments (1 sun AM1.5G irradiation, 50% RH, 50 °C device temperature), such cells engaged more than 80% of their early photovoltaic performance after 50 h and worked stably for the next 135 h.[236]

A two-sided border alteration to perovskites by doping with $CsPbBr_3$ nanocrystals (CN) was also described. It was found that CN efficiently overcomes the flaw at the $SnO_2$/perovskite border and improves the interfacial electron transfer.[237] Furthermore, by introducing the hybrid density functional theory (DFT) based simulations, an interface was created between the fluorinated Zn-phthalocyanine (FnZnPc) and $MAPbI_3$ surface. It was observed that FnZnPc procedures a steady boundary with the $MAPbI_3$ surface with obligatory energies compared to the unsubstituted case.[238]

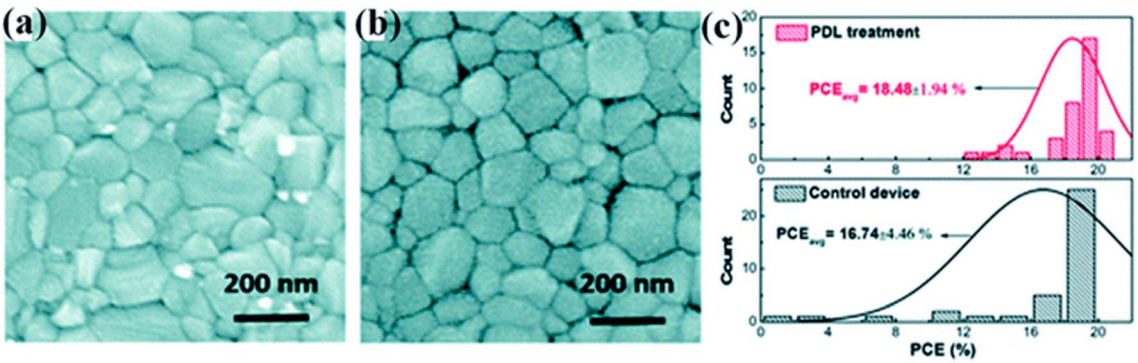


Fig. 31 SEM top view pictures of perovskite thin layers (a) without any treatment and (b) with post-device ligand treatment. (c) Histograms of the device efficiencies with PDL treatment and without any treatment (37 cells were made-up and verified, reproduced with permission from ref. 225. Copyright 2018 Elsevier).


© 2023 The Author(s). Published by the Royal Society of Chemistry

Open Access Article. Published on 02 1402. Downloaded on 14/11/1404 12:16:38 ..
This article is licensed under a Creative Commons Attribution-NonCommercial 3.0 Unported Licence.

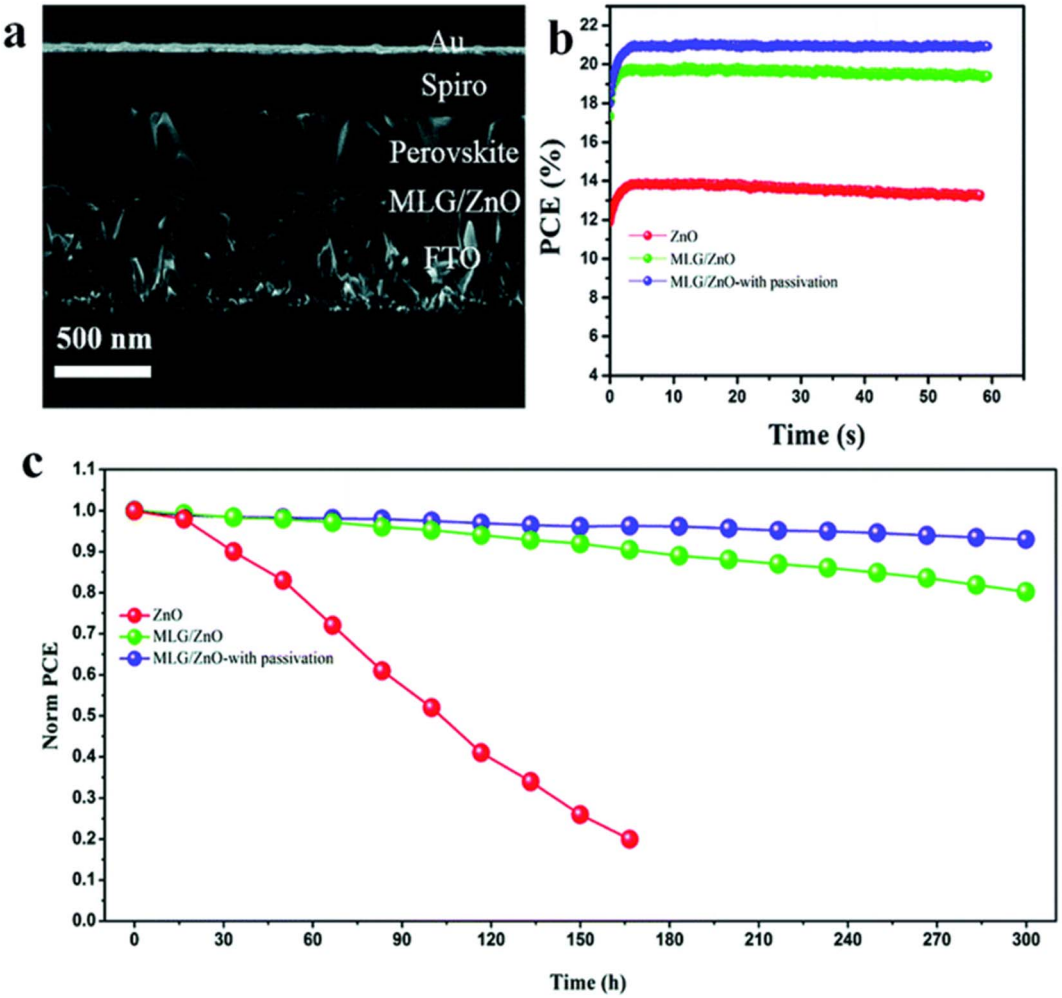


Fig. 32 (a) Side view SEM image of the PSC fabricated using MLG/ZnO. (b) PCE curve with time under maximum power point tracking. (c) Stability test of PSCs based on ZnO, MLG/ZnO, and MLG/ZnO with passivation under constant illumination for 300 hours at room temperature and under nitrogen flow (reproduced with permission from ref. 235. Copyright 2019 RSC).

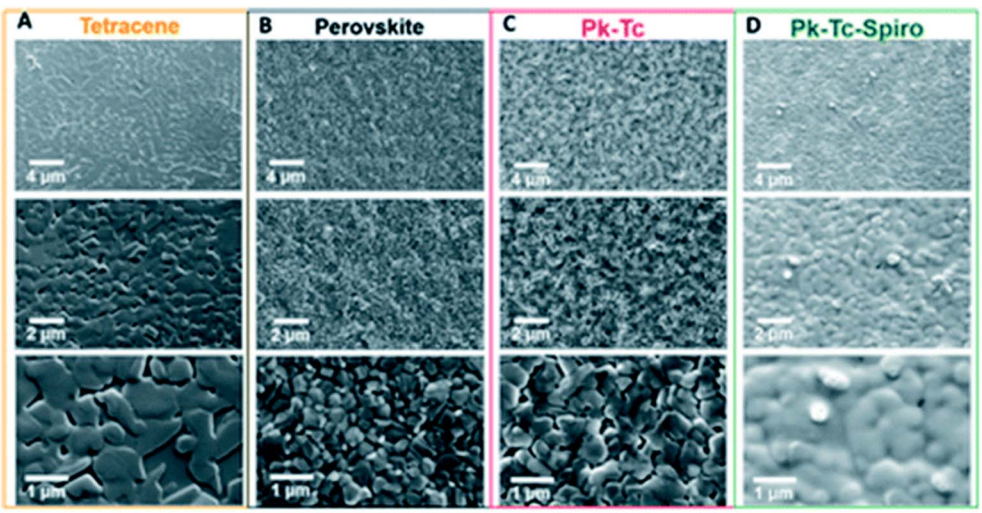


Fig. 33 Top-view scanning electron microscopy of (A) tetracene (Tc) single coat, (B) perovskite (Pk), (C) perovskite–tetracene (Pk–Tc), and (D) perovskite–tetracene–Spiro (Pk–Tc–Spiro) layers at three diverse magnifications (reproduced with permission from ref. 236. Copyright 2019 AAAS).

Open Access Article. Published on 02 1402. Downloaded on 14/11/1404 12:16:38 ..
This article is licensed under a Creative Commons Attribution-NonCommercial 3.0 Unported Licence.

## 6. Conclusions

Since the progress of solid-state perovskite solar cells in 2012, the efficiency of these devices has offered an extraordinarily swift improvement from 9.7% to 25.2% in less than 10 years. Initiated by the advancement of the perovskite solar cell in 2012, profound development in structure scheme, materials understanding, method engineering, and device physics has paid to the innovatory advancement of the perovskite solar cell to be a robust contestant for a next-generation solar energy mower. The superior efficiency together with the inexpensive materials and procedures are the trade points of these devices over profit-making silicon or other inorganic and organic solar cells. Since an extraordinary performance is directly connected to the device arrangement, understanding the device dynamics and device construction engineering is of dire significance, although, the interfaces and materials used in the perovskite devices are similarly vital for attaining maximum device performance. On the other hand, an optimum fabrication procedure must be established, precisely for excellent perovskite films, since the perovskite light absorber is the crucial component in the perovskite devices. Moreover, the growth of low-bandgap perovskite materials built on a Sn/Pb diverse composition has made it conceivable to construct perovskite/perovskite tandem solar cells. Modifying the bandgap of these materials, while reducing the possible damage, will ease extra improvements in the efficiency to >30%. Investigations on perovskite devices are continuing, and it is predictable that they will show an important part in the upcoming solar energy. It is vital to (1) produce effective and stable perovskite materials, (2) participate in emerging suitable tools and procedures for making mini-modules, (3) launch close partnerships between companies and academia to report the persistent matters in emerging large-sized cells, and (4) introduce vigorous testing measures to precisely measure the long-term steadiness of perovskites.

## Conflicts of interest

There are no conflicts to declare.

## Acknowledgements

The authors gratefully acknowledge the financial support from the Higher Education Commission (HEC) of Pakistan.

## References

1 Q. Wang, *et al.*, Progress in emerging solution-processed thin film solar cells–Part I: Polymer solar cells, *Renewable Sustainable Energy Rev.*, 2016, **56**, 347–361.
2 J. Jaksik, *et al.*, Nanostructured functional materials for advanced three-dimensional (3D) solar cells, *Sol. Energy Mater. Sol. Cells*, 2017, **167**, 121–132.
3 J. Mohtasham, Renewable energies, *Energy Procedia*, 2015, **74**, 1289–1297.
4 O. Ellabban, H. Abu-Rub and F. Blaabjerg, Renewable energy resources: Current status, future prospects and their enabling technology, *Renewable Sustainable Energy Rev.*, 2014, **39**, 748–764.
5 N. S. Lewis, Toward cost-effective solar energy use, *science*, 2007, **315**(5813), 798–801.
6 M. Green, *et al.*, Solar cell efficiency tables (version 57), *Prog. Photovolt.: Res. Appl.*, 2021, **29**(1), 3–15.
7 J. Euvrard, Y. Yan and D. B. Mitzi, Electrical doping in halide perovskites, *Nat. Rev. Mater.*, 2021, **6**(6), 531–549.
8 D. Weber, $CH_3NH_3PbX_3$, ein Pb (II)-system mit kubischer perowskitstruktur/$CH_3NH_3PbX_3$, a Pb (II)-system with cubic perovskite structure, *Z. Naturforsch. B*, 1978, **33**(12), 1443–1445.
9 D. Weber, $CH_3NH_3SnBr_xI_{3-x}$ ($x$ = 0–3), ein Sn (II)-System mit kubischer Perowskitstruktur/$CH_3NH_3SnBr_xI_{3-x}$ ($x$= 0–3), a Sn (II)-system with cubic perovskite structure, *Z. Naturforsch. B*, 1978, **33**(8), 862–865.
10 L. Li and M. Yan, Recent progress in the development of RE2TMTM′O6 double perovskite oxides for cryogenic magnetic refrigeration, *J. Mater. Sci. Technol.*, 2023, **136**, 1–12.
11 D. Mitzi, *et al.*, Conducting layered organic-inorganic halides containing ⟨110⟩-oriented perovskite sheets, *Science*, 1995, **267**(5203), 1473–1476.
12 A. Kojima, *et al.*, Organometal halide perovskites as visible-light sensitizers for photovoltaic cells, *J. Am. Chem. Soc.*, 2009, **131**(17), 6050–6051.
13 G. Yu, *et al.*, Polymer photovoltaic cells: enhanced efficiencies *via* a network of internal donor–acceptor heterojunctions, *Science*, 1995, **270**(5243), 1789–1791.
14 J. Xu, *et al.*, Efficiently photo-charging lithium-ion battery by perovskite solar cell, *Nat. Commun.*, 2015, **6**(1), 1–7.
15 Q. Dong, *et al.*, Electron-hole diffusion lengths >175 μm in solution-grown $CH_3NH_3PbI_3$ single crystals, *Science*, 2015, **347**(6225), 967–970.
16 L. P. Lekesi, *et al.*, Developments on Perovskite Solar Cells (PSCs): A Critical Review, *Appl. Sci.*, 2022, **12**(2), 672.
17 V. D'innocenzo, *et al.*, Excitons *versus* free charges in organo-lead tri-halide perovskites, *Nat. Commun.*, 2014, **5**(1), 1–6.
18 M. Saba, *et al.*, Excited state properties of hybrid perovskites, *Acc. Chem. Res.*, 2016, **49**(1), 166–173.
19 F. Giustino and H. J. Snaith, Toward lead-free perovskite solar cells, *ACS Energy Lett.*, 2016, **1**(6), 1233–1240.
20 L. De Marco, *et al.*, Perovskite Single-Crystal Solar Cells: Advances and Challenges, *Sol. RRL*, 2022, **6**(7), 2101085.
21 T. A. Berhe, *et al.*, Organometal halide perovskite solar cells: degradation and stability, *Energy Environ. Sci.*, 2016, **9**(2), 323–356.
22 S. Yang, *et al.*, Recent advances in perovskite solar cells: efficiency, stability and lead-free perovskite, *J. Mater. Chem. A*, 2017, **5**(23), 11462–11482.
23 Z. Chchiyai, *et al.*, Effect of cobalt doping on the crystal structure, magnetic, dielectric, electrical and optical properties of $PbTi_{1-x}Co_xO_{3-\delta}$ perovskite materials, *J. Alloys Compd.*, 2022, **927**, 166979.


© 2023 The Author(s). Published by the Royal Society of Chemistry

Open Access Article. Published on 02 1402. Downloaded on 14/11/1404 12:16:38 ..
This article is licensed under a Creative Commons Attribution-NonCommercial 3.0 Unported Licence.

24 M. Habibi, *et al.*, Progress in emerging solution-processed thin film solar cells–Part II: Perovskite solar cells, *Renewable Sustainable Energy Rev.*, 2016, **62**, 1012–1031.
25 N.-G. Park, Perovskite solar cells: an emerging photovoltaic technology, *Mater. Today*, 2015, **18**(2), 65–72.
26 C. Li, *et al.*, Formability of abx3 (x= f, cl, br, i) halide perovskites, *Acta Crystallogr., Sect. B: Struct. Sci.*, 2008, **64**(6), 702–707.
27 V. M. Goldschmidt, Die gesetze der krystallochemie, *Naturwissenschaften*, 1926, **14**(21), 477–485.
28 M. A. Green, A. Ho-Baillie and H. J. Snaith, The emergence of perovskite solar cells, *Nat. Photonics*, 2014, **8**(7), 506–514.
29 M. Asghar, *et al.*, Device stability of perovskite solar cells–A review, *Renewable Sustainable Energy Rev.*, 2017, **77**, 131–146.
30 J. Chen and N.-G. Park, Inorganic hole transporting materials for stable and high efficiency perovskite solar cells, *J. Phys. Chem. C*, 2018, **122**(25), 14039–14063.
31 H. Fujiwara, *Hybrid Perovskite Solar Cells: Characteristics and Operation*, John Wiley & Sons, 2022.
32 N. Marinova, S. Valero and J. L. Delgado, Organic and perovskite solar cells: Working principles, materials and interfaces, *J. Colloid Interface Sci.*, 2017, **488**, 373–389.
33 H.-S. Kim, *et al.*, Lead iodide perovskite sensitized all-solid-state submicron thin film mesoscopic solar cell with efficiency exceeding 9%, *Sci. Rep.*, 2012, **2**(1), 1–7.
34 H. Zhou, *et al.*, Interface engineering of highly efficient perovskite solar cells, *Science*, 2014, **345**(6196), 542–546.
35 Z. Song, *et al.*, Perovskite solar cells go bifacial—mutual benefits for efficiency and durability, *Adv. Mater.*, 2022, **34**(4), 2106805.
36 Z. Song, *et al.*, Pathways toward high-performance perovskite solar cells: review of recent advances in organo-metal halide perovskites for photovoltaic applications, *J. Photonics Energy*, 2016, **6**(2), 022001.
37 J. Wei, *et al.*, Hysteresis analysis based on the ferroelectric effect in hybrid perovskite solar cells, *J. Phys. Chem. Lett.*, 2014, **5**(21), 3937–3945.
38 H.-S. Kim, *et al.*, Control of *I–V* hysteresis in $CH_3NH_3PbI_3$ perovskite solar cell, *J. Phys. Chem. Lett.*, 2015, **6**(22), 4633–4639.
39 B. Chen, *et al.*, Origin of *J–V* hysteresis in perovskite solar cells, *J. Phys. Chem. Lett.*, 2016, **7**(5), 905–917.
40 Z. Shi and A. H. Jayatissa, Perovskites-based solar cells: A review of recent progress, materials and processing methods, *Materials*, 2018, **11**(5), 729.
41 L. Yin, *et al.*, Functionalized-MXene-nanosheet-doped tin oxide enhances the electrical properties in perovskite solar cells, *Cell Rep. Phys. Sci.*, 2022, **3**(6), 100905.
42 L. Meng, *et al.*, Recent advances in the inverted planar structure of perovskite solar cells, *Acc. Chem. Res.*, 2016, **49**(1), 155–165.
43 J. Y. Jeng, *et al.*, $CH_3NH_3PbI_3$ perovskite/fullerene planar-heterojunction hybrid solar cells, *Adv. Mater.*, 2013, **25**(27), 3727–3732.
44 L. Etgar, *et al.*, Mesoscopic $CH_3NH_3PbI_3/TiO_2$ heterojunction solar cells, *J. Am. Chem. Soc.*, 2012, **134**(42), 17396–17399.
45 Y. Yang, *et al.*, Perovskite Solar Cells Based Self-Charging Power Packs Fundamentals, Applications and Challenges, *Nano Energy*, 2022, 106910.
46 L. Huang, *et al.*, Toward revealing the critical role of perovskite coverage in highly efficient electron-transport layer-free perovskite solar cells: an energy band and equivalent circuit model perspective, *ACS Appl. Mater. Interfaces*, 2016, **8**(15), 9811–9820.
47 Q. Hu, *et al.*, Engineering of electron-selective contact for perovskite solar cells with efficiency exceeding 15, *ACS Nano*, 2014, **8**(10), 10161–10167.
48 W. Ke, *et al.*, Efficient hole-blocking layer-free planar halide perovskite thin-film solar cells, *Nat. Commun.*, 2015, **6**(1), 1–7.
49 D. Prochowicz, *et al.*, Mechanosynthesis of pure phase mixed-cation $MA_xFA_{1-x}$ $PbI_3$ hybrid perovskites: photovoltaic performance and electrochemical properties, *Sustainable Energy Fuels*, 2017, **1**(4), 689–693.
50 W. S. Yang, *et al.*, High-performance photovoltaic perovskite layers fabricated through intramolecular exchange, *Science*, 2015, **348**(6240), 1234–1237.
51 D. M. Jang, *et al.*, Reversible halide exchange reaction of organometal trihalide perovskite colloidal nanocrystals for full-range band gap tuning, *Nano Lett.*, 2015, **15**(8), 5191–5199.
52 W.-J. Yin, *et al.*, Halide perovskite materials for solar cells: a theoretical review, *J. Mater. Chem. A*, 2015, **3**(17), 8926–8942.
53 L. Huang, *et al.*, Efficient planar perovskite solar cells without a high temperature processed titanium dioxide electron transport layer, *Sol. Energy Mater. Sol. Cells*, 2016, **149**, 1–8.
54 J. W. Lee, *et al.*, High-efficiency perovskite solar cells based on the black polymorph of $HC(NH_2)2PbI_3$, *Adv. Mater.*, 2014, **26**(29), 4991–4998.
55 Q. Zhu, *et al.*, Compact layer free perovskite solar cells with a high-mobility hole-transporting layer, *ACS Appl. Mater. Interfaces*, 2016, **8**(4), 2652–2657.
56 S. Aharon, *et al.*, Depletion region effect of highly efficient hole conductor free $CH_3$ $NH_3$ $PbI_3$ perovskite solar cells, *Phys. Chem. Chem. Phys.*, 2014, **16**(22), 10512–10518.
57 F. C. Hanusch, *et al.*, Efficient planar heterojunction perovskite solar cells based on formamidinium lead bromide, *J. Phys. Chem. Lett.*, 2014, **5**, 2791–2795.
58 N. J. Jeon, *et al.*, Compositional engineering of perovskite materials for high-performance solar cells, *Nature*, 2015, **517**(7535), 476–480.
59 N. Pellet, *et al.*, Mixed-organic-cation Perovskite photovoltaics for enhanced solar-light harvesting, *Angew. Chem.*, 2014, **126**(12), 3215–3221.
60 J.-P. Correa-Baena, *et al.*, The rapid evolution of highly efficient perovskite solar cells, *Energy Environ. Sci.*, 2017, **10**(3), 710–727.

Open Access Article. Published on 02 1402. Downloaded on 14/11/1404 12:16:38 ..
This article is licensed under a Creative Commons Attribution-NonCommercial 3.0 Unported Licence.

61 M. Saliba, *et al.*, Incorporation of rubidium cations into perovskite solar cells improves photovoltaic performance, *Science*, 2016, **354**(6309), 206–209.
62 M. Saliba, *et al.*, Cesium-containing triple cation perovskite solar cells: improved stability, reproducibility and high efficiency, *Energy Environ. Sci.*, 2016, **9**(6), 1989–1997.
63 H. Choi, *et al.*, Cesium-doped methylammonium lead iodide perovskite light absorber for hybrid solar cells, *Nano Energy*, 2014, **7**, 80–85.
64 Y. Liu, *et al.*, Two-inch-sized perovskite $CH_3NH_3PbX_3$ (X = Cl, Br, I) crystals: growth and characterization, *Adv. Mater.*, 2015, **27**(35), 5176–5183.
65 B. Suarez, *et al.*, Recombination study of combined halides (Cl, Br, I) perovskite solar cells, *J. Phys. Chem. Lett.*, 2014, **5**(10), 1628–1635.
66 E. Edri, *et al.*, Chloride inclusion and hole transport material doping to improve methyl ammonium lead bromide perovskite-based high open-circuit voltage solar cells, *J. Phys. Chem. Lett.*, 2014, **5**(3), 429–433.
67 S. Seo, *et al.*, An ultra-thin, un-doped NiO hole transporting layer of highly efficient (16.4%) organic–inorganic hybrid perovskite solar cells, *Nanoscale*, 2016, **8**(22), 11403–11412.
68 M. M. Lee, *et al.*, Efficient hybrid solar cells based on meso-superstructured organometal halide perovskites, *Science*, 2012, **338**(6107), 643–647.
69 J. H. Noh, *et al.*, Chemical management for colorful, efficient, and stable inorganic–organic hybrid nanostructured solar cells, *Nano Lett.*, 2013, **13**(4), 1764–1769.
70 H. Choi, *et al.*, Cesium-doped methylammonium lead iodide perovskite light absorber for hybrid solar cells, *Nano Energy*, 2014, **7**, 80–85.
71 T. J. Jacobsson, *et al.*, Exploration of the compositional space for mixed lead halogen perovskites for high efficiency solar cells, *Energy Environ. Sci.*, 2016, **9**(5), 1706–1724.
72 N. K. Noel, *et al.*, Lead-free organic–inorganic tin halide perovskites for photovoltaic applications, *Energy Environ. Sci.*, 2014, **7**(9), 3061–3068.
73 W.-J. Yin, Y. Yan and S.-H. Wei, Anomalous alloy properties in mixed halide perovskites, *J. Phys. Chem. Lett.*, 2014, **5**(21), 3625–3631.
74 E. H. Anaraki, *et al.*, Highly efficient and stable planar perovskite solar cells by solution-processed tin oxide, *Energy Environ. Sci.*, 2016, **9**(10), 3128–3134.
75 A. Sharma, A comprehensive study of solar power in India and World, *Renewable Sustainable Energy Rev.*, 2011, **15**(4), 1767–1776.
76 N. Kannan and D. Vakeesan, Solar energy for future world:- A review, *Renewable Sustainable Energy Rev.*, 2016, **62**, 1092–1105.
77 B. W. Park, *et al.*, Bismuth based hybrid perovskites A3Bi2I9 (A: methylammonium or cesium) for solar cell application, *Adv. 2D Mater.*, 2015, **27**(43), 6806–6813.
78 S. Sen, *et al.*, Renewable energy scenario in India: Opportunities and challenges, *J. Afr. Earth Sci.*, 2016, **122**, 25–31.
79 A. Kumar, *et al.*, Renewable energy in India: current status and future potentials, *Renewable Sustainable Energy Rev.*, 2010, **14**(8), 2434–2442.
80 H. Tang, S. He and C. Peng, A short progress report on high-efficiency perovskite solar cells, *Nanoscale Res. Lett.*, 2017, **12**(1), 1–8.
81 K. Kaygusuz, Energy for sustainable development: key issues and challenges, *Energy Sources, Part B*, 2007, **2**(1), 73–83.
82 Z. Wang, *et al.*, Stability of perovskite solar cells: a prospective on the substitution of the A cation and X anion, *Angew. Chem., Int. Ed.*, 2017, **56**(5), 1190–1212.
83 J. Gong, C. Li and M. R. Wasielewski, Advances in solar energy conversion, *Chem. Soc. Rev.*, 2019, **48**(7), 1862–1864.
84 M. B. Hayat, *et al.*, Solar energy—A look into power generation, challenges, and a solar-powered future, *Int. J. Energy Res.*, 2019, **43**(3), 1049–1067.
85 E. Kabir, *et al.*, Solar energy: Potential and future prospects, *Renewable Sustainable Energy Rev.*, 2018, **82**, 894–900.
86 H. J. Snaith, Perovskites: the emergence of a new era for low-cost, high-efficiency solar cells, *J. Phys. Chem. Lett.*, 2013, **4**(21), 3623–3630.
87 R. Wang, *et al.*, A review of perovskites solar cell stability, *Adv. Funct. Mater.*, 2019, **29**(47), 1808843.
88 S. K. Hau, H.-L. Yip and A. K.-Y. Jen, A review on the development of the inverted polymer solar cell architecture, *Polym. Rev.*, 2010, **50**(4), 474–510.
89 A. M. Humada, *et al.*, Solar cell parameters extraction based on single and double-diode models: A review, *Renewable Sustainable Energy Rev.*, 2016, **56**, 494–509.
90 P. K. Nayak, *et al.*, Photovoltaic solar cell technologies: analysing the state of the art, *Nat. Rev. Mater.*, 2019, **4**(4), 269–285.
91 A. Kumar, *et al.*, Efficient and stable perovskite solar cells by interface engineering at the interface of electron transport layer/perovskite, *Opt. Mater.*, 2022, **132**, 112846.
92 J. Gong, *et al.*, Review on dye-sensitized solar cells (DSSCs): Advanced techniques and research trends, *Renewable Sustainable Energy Rev.*, 2017, **68**, 234–246.
93 N. A. Ludin, *et al.*, Review on the development of natural dye photosensitizer for dye-sensitized solar cells, *Renewable Sustainable Energy Rev.*, 2014, **31**, 386–396.
94 Z. Hu, *et al.*, A critical review on semitransparent organic solar cells, *Nano Energy*, 2020, **78**, 105376.
95 J. Yan and B. R. Saunders, Third-generation solar cells: a review and comparison of polymer: fullerene, hybrid polymer and perovskite solar cells, *RSC Adv.*, 2014, **4**(82), 43286–43314.
96 P. Zhao, B. J. Kim and H. S. Jung, Passivation in perovskite solar cells: A review, *Mater. Today Energy*, 2018, **7**, 267–286.
97 A. Raj, *et al.*, Evidence of improved power conversion efficiency in lead-free CsGeI3 based perovskite solar cell heterostructure *via* scaps simulation, *J. Vac. Sci. Technol. B:Nanotechnol. Microelectron.*, 2021, **39**(1), 012401.
98 M. Kumar, *et al.*, Theoretical evidence of high power conversion efficiency in double perovskite solar cell device, *Opt. Mater.*, 2021, **111**, 110565.


© 2023 The Author(s). Published by the Royal Society of Chemistry

Open Access Article. Published on 02 1402. Downloaded on 14/11/1404 12:16:38 ..
This article is licensed under a Creative Commons Attribution-NonCommercial 3.0 Unported Licence.

99 L. Chu, Pseudohalide anion engineering for highly efficient and stable perovskite solar cells, *Matter*, 2021, **4**(6), 1762–1764.
100 S. Bai, *et al.*, Planar perovskite solar cells with long-term stability using ionic liquid additives, *Nature*, 2019, **571**(7764), 245–250.
101 V. Zardetto, *et al.*, Atomic layer deposition for perovskite solar cells: research status, opportunities and challenges, *Sustainable Energy Fuels*, 2017, **1**(1), 30–55.
102 M. I. H. Ansari, A. Qurashi and M. K. Nazeeruddin, Frontiers, opportunities, and challenges in perovskite solar cells: A critical review, *J. Photochem. Photobiol.*, 2018, **35**, 1–24.
103 S. Ravishankar, *et al.*, Influence of Charge Transport Layers on Open-Circuit Voltage and Hysteresis in Perovskite Solar Cells, *Joule*, 2018, **2**(4), 788–798.
104 A. K. Al-Mousoi, *et al.*, Simulation and analysis of lead-free perovskite solar cells incorporating cerium oxide as electron transporting layer, *RSC Adv.*, 2022, **12**(50), 32365–32373.
105 P. Docampo, *et al.*, Efficient organometal trihalide perovskite planar-heterojunction solar cells on flexible polymer substrates, *Nat. Commun.*, 2013, **4**(1), 1–6.
106 Y.-F. Chiang, *et al.*, High voltage and efficient bilayer heterojunction solar cells based on an organic–inorganic hybrid perovskite absorber with a low-cost flexible substrate, *Phys. Chem. Chem. Phys.*, 2014, **16**(13), 6033–6040.
107 N. Akhtar, *et al.*, Self-Assembly of Ferromagnetic Organic–Inorganic Perovskite-Like Films, *Small*, 2014, **10**(23), 4912–4919.
108 (*a*) J. Heo, *et al.*, *Nat. Photonics*, 2013, **7**, 486; (*b*) N. J. Jeon, J. H. Noh, Y. C. Kim, W. S. Yang and S. Ryu, *Nat. Mater*, 2014, **13**, 897.
109 (*a*) S. Bai, *et al.*, *Nano Res.*, 2014, **7**, 1749; (*b*) J. Jeng, Y. Chiang, M. Lee, S. Peng, T. Guo, P. Chen and T. Wen, *Adv. Mater.*, 2013, **25**, 3727.
110 G. Giorgi, *et al.*, Small photocarrier effective masses featuring ambipolar transport in methylammonium lead iodide perovskite: a density functional analysis, *J. Phys. Chem. Lett.*, 2013, **4**(24), 4213–4216.
111 E. E. Chufán, S. C. Puiu and K. D. Karlin, Heme–copper/dioxygen adduct formation, properties, and reactivity, *Acc. Chem. Res.*, 2007, **40**(7), 563–572.
112 D.-X. Yuan, *et al.*, Inverted planar NH 2 CH [double bond, length as m-dash] $NH_2$ $PbI_3$ perovskite solar cells with 13.56% efficiency *via* low temperature processing, *Phys. Chem. Chem. Phys.*, 2015, **17**(30), 19745–19750.
113 W. Xu, *et al.*, Perovskite hybrid solar cells with a fullerene derivative electron extraction layer, *J. Mater. Chem. C*, 2017, **5**(17), 4190–4197.
114 T. Zhang, *et al.*, Recent progress in improving strategies of inorganic electron transport layers for perovskite solar cells, *Nano Energy*, 2022, 107918.
115 H. S. Jung and N. G. Park, Perovskite solar cells: from materials to devices, *Small*, 2015, **11**(1), 10–25.
116 S. D. Stranks and H. J. Snaith, Metal-halide perovskites for photovoltaic and light-emitting devices, *Nat. Nanotechnol.*, 2015, **10**(5), 391–402.
117 H. Liu, *et al.*, Fabrication of InGaZnO-$SnO_2$/PCBM hybrid electron transfer layer for high-performance Perovskite solar cell and X-ray detector, *J. Alloys Compd.*, 2022, **906**, 164399.
118 G. Yang, *et al.*, Recent progress in electron transport layers for efficient perovskite solar cells, *J. Mater. Chem. A*, 2016, **4**(11), 3970–3990.
119 J. Zhang, *et al.*, Amino-Functionalized Niobium-Carbide MXene Serving as Electron Transport Layer and Perovskite Additive for the Preparation of High-Performance and Stable Methylammonium-Free Perovskite Solar Cells, *Adv. Funct. Mater.*, 2022, **32**(24), 2113367.
120 A. K. Jena, A. Kulkarni and T. Miyasaka, Halide perovskite photovoltaics: background, status, and future prospects, *Chem. Rev.*, 2019, **119**(5), 3036–3103.
121 L. Qiu, *et al.*, Scalable fabrication of metal halide perovskite solar cells and modules, *ACS Energy Lett.*, 2019, **4**(9), 2147–2167.
122 H.-S. Kim, S. H. Im and N.-G. Park, Organolead halide perovskite: new horizons in solar cell research, *J. Phys. Chem. C*, 2014, **118**(11), 5615–5625.
123 Q. Fu, *et al.*, Amphiphilic fullerenes employed to improve the quality of perovskite films and the stability of perovskite solar cells, *ACS Appl. Mater. Interfaces*, 2019, **11**(27), 24782–24788.
124 B. Yang, *et al.*, Highly efficient semitransparent $CsPbIBr_2$ perovskite solar cells *via* low-temperature processed $In_2S_3$ as electron-transport-layer, *Nano Energy*, 2019, **57**, 718–727.
125 X. Xu, *et al.*, Enhanced detectivity and suppressed dark current of Perovskite–InGaZnO phototransistor *via* a PCBM interlayer, *ACS Appl. Mater. Interfaces*, 2018, **10**(50), 44144–44151.
126 H.-S. Lin, *et al.*, Achieving high efficiency in solution-processed perovskite solar cells using $C_{60}$/$C_{70}$ mixed fullerenes, *ACS Appl. Mater. Interfaces*, 2018, **10**(46), 39590–39598.
127 M. K. Mohammed, *et al.*, Ionic liquid passivator for mesoporous titanium dioxide electron transport layer to enhance the efficiency and stability of hole conductor-free perovskite solar cells, *Energy Fuels*, 2022, **36**(19), 12192–12200.
128 H. Chen, *et al.*, Er and Mg co-doped $TiO_2$ nanorod arrays and improvement of photovoltaic property in perovskite solar cell, *J. Alloys Compd.*, 2019, **771**, 649–657.
129 A. Seitkhan, *et al.*, A multilayered electron extracting system for efficient perovskite solar cells, *Adv. Funct. Mater.*, 2020, **30**(43), 2004273.
130 S. K. Jung, *et al.*, Non-Fullerene Organic Electron-Transporting Materials for Perovskite Solar Cells, *ChemSusChem*, 2018, **11**(22), 3882–3892.
131 M. A. Uddin, *et al.*, Blading of Conformal Electron-Transport Layers in p–i–n Perovskite Solar Cells, *Adv. Mater.*, 2022, **34**(30), 2202954.

Open Access Article. Published on 02 1402. Downloaded on 14/11/1404 12:16:38 ..
This article is licensed under a Creative Commons Attribution-NonCommercial 3.0 Unported Licence.

132 R. Singh, *et al.*, Review of current progress in inorganic hole-transport materials for perovskite solar cells, *Appl. Mater. Today*, 2019, **14**, 175–200.
133 H. Liu, *et al.*, Nano-structured electron transporting materials for perovskite solar cells, *Nanoscale*, 2016, **8**(12), 6209–6221.
134 R. Teimouri, *et al.*, Synthesizing Li doped $TiO_2$ electron transport layers for highly efficient planar perovskite solar cell, *Superlattices Microstruct.*, 2020, **145**, 106627.
135 Q. Cai, *et al.*, Enhancing efficiency of planar structure perovskite solar cells using Sn-doped $TiO_2$ as electron transport layer at low temperature, *Electrochim. Acta*, 2018, **261**, 227–235.
136 S. Wang, *et al.*, Enhanced performance of $TiO_2$-based perovskite solar cells with Ru-doped $TiO_2$ electron transport layer, *Sol. Energy*, 2018, **169**, 335–342.
137 Z. Li, *et al.*, Annealing free tin oxide electron transport layers for flexible perovskite solar cells, *Nano Energy*, 2022, **94**, 106919.
138 Y. Wang, *et al.*, A rutile $TiO_2$ electron transport layer for the enhancement of charge collection for efficient perovskite solar cells, *Angew. Chem., Int. Ed.*, 2019, **58**(28), 9414–9418.
139 D. Zhong, *et al.*, Synthesis of oriented $TiO_2$ nanocones with fast charge transfer for perovskite solar cells, *Nano Energy*, 2015, **11**, 409–418.
140 F. Biccari, *et al.*, Graphene-based electron transport layers in perovskite solar cells: a step-up for an efficient carrier collection, *Adv. Energy Mater.*, 2017, **7**(22), 1701349.
141 L. Zuo, *et al.*, Enhanced photovoltaic performance of $CH_3NH_3PbI_3$ perovskite solar cells through interfacial engineering using self-assembling monolayer, *J. Am. Chem. Soc.*, 2015, **137**(7), 2674–2679.
142 W. Zhao, *et al.*, Comprehensive investigation of sputtered and spin-coated zinc oxide electron transport layers for highly efficient and stable planar perovskite solar cells, *J. Power Sources*, 2019, **427**, 223–230.
143 D. Liu and T. L. Kelly, Perovskite solar cells with a planar heterojunction structure prepared using room-temperature solution processing techniques, *Nat. Photonics*, 2014, **8**(2), 133–138.
144 S. Huang, *et al.*, Modification of $SnO_2$ electron transport Layer: Brilliant strategies to make perovskite solar cells stronger, *Chem. Eng. J.*, 2022, 135687.
145 K. Mahmood, B. S. Swain and A. Amassian, Double-layered ZnO nanostructures for efficient perovskite solar cells, *Nanoscale*, 2014, **6**(24), 14674–14678.
146 L. Wang, *et al.*, Indium Zinc Oxide Electron Transport Layer for High-Performance Planar Perovskite Solar Cells, *J. Phys. Chem. C*, 2018, **122**(50), 28491–28496.
147 J. Cao, *et al.*, Efficient, hysteresis-free, and stable perovskite solar cells with ZnO as electron-transport layer: effect of surface passivation, *Adv. Mater.*, 2018, **30**(11), 1705596.
148 Y. Li, *et al.*, Mesoporous $SnO_2$ nanoparticle films as electron-transporting material in perovskite solar cells, *RSC Adv.*, 2015, **5**, 28424–28429.
149 Q. Dong, *et al.*, Insight into perovskite solar cells based on $SnO_2$ compact electron-selective layer, *J. Phys. Chem. C*, 2015, **119**(19), 10212–10217.
150 K. Choi, *et al.*, Thermally stable, planar hybrid perovskite solar cells with high efficiency, *Energy Environ. Sci.*, 2018, **11**(11), 3238–3247.
151 J. J. Yoo, *et al.*, Efficient perovskite solar cells *via* improved carrier management, *Nature*, 2021, **590**(7847), 587–593.
152 W. Ke, *et al.*, Efficient planar perovskite solar cells using room-temperature vacuum-processed $C_{60}$ electron selective layers, *J. Mater. Chem. A*, 2015, **3**, 17971–17976.
153 H. Yoon, *et al.*, Hysteresis-free low-temperature-processed planar perovskite solar cells with 19.1% efficiency, *Energy Environ. Sci.*, 2016, **9**(7), 2262–2266.
154 C. Xu, *et al.*, High-performance inverted planar perovskite solar cells using a pristine fullerene mixture as an electron-transport layer, *J. Mater. Chem. C*, 2019, **7**, 6956–6963.
155 J. Pascual, *et al.*, Electron Transport Layer-Free Solar Cells Based on Perovskite–Fullerene Blend Films with Enhanced Performance and Stability, *ChemSusChem*, 2016, **9**(18), 2679–2685.
156 X. Zeng, *et al.*, Performance improvement of perovskite solar cells by employing a CdSe quantum dot/PCBM composite as an electron transport layer, *J. Mater. Chem. A*, 2017, **5**(33), 17499–17505.
157 J. Seo, *et al.*, Benefits of very thin PCBM and LiF layers for solution-processed p–i–n perovskite solar cells, *Energy Environ. Sci.*, 2014, **7**(8), 2642–2646.
158 F. Guo, *et al.*, High-performance semitransparent perovskite solar cells with solution-processed silver nanowires as top electrodes, *Nanoscale*, 2015, **7**(5), 1642–1649.
159 J. Xie, *et al.*, A ternary organic electron transport layer for efficient and photostable perovskite solar cells under full spectrum illumination, *J. Mater. Chem. A*, 2018, **6**(14), 5566–5573.
160 C. Li, *et al.*, A PCBM-assisted perovskite growth process to fabricate high efficiency semitransparent solar cells, *J. Mater. Chem. A*, 2016, **4**(30), 11648–11655.
161 Y. Zhong, *et al.*, Role of PCBM in the suppression of hysteresis in perovskite solar cells, *Adv. Funct. Mater.*, 2020, **30**(23), 1908920.
162 Y. Fan, *et al.*, A perylene diimide dimer-based electron transporting material with an A–D–A structure for efficient inverted perovskite solar cells, *J. Mater. Chem. C*, 2022, **10**(7), 2544–2550.
163 H. Zhang, *et al.*, New generation perovskite solar cells with solution-processed amino-substituted perylene diimide derivative as electron-transport layer, *J. Mater. Chem. A*, 2016, **4**(22), 8724–8733.
164 P. Karuppuswamy, *et al.*, Solution-processable electron transport layer for efficient hybrid perovskite solar cells beyond fullerenes, *Sol. Energy Mater. Sol. Cells*, 2017, **169**, 78–85.
165 G. S. Perez, *et al.*, Solution-processable perylene diimide-based electron transport materials as non-fullerene


© 2023 The Author(s). Published by the Royal Society of Chemistry

Open Access Article. Published on 02 1402. Downloaded on 14/11/1404 12:16:38 ..
This article is licensed under a Creative Commons Attribution-NonCommercial 3.0 Unported Licence.

alternatives for inverted perovskite solar cells, *J. Mater. Chem. A*, 2022, **10**(20), 11046–11053.
166 I. Hussain, *et al.*, Functional materials, device architecture, and flexibility of perovskite solar cell, *Emergent Mater.*, 2018, **1**, 133–154.
167 Z. Xing, *et al.*, Crystallographic understanding of photoelectric properties for C 60 derivatives applicable as electron transporting materials in perovskite solar cells, *Chem. Res. Chin. Univ.*, 2022, 1–7.
168 T. Qin, *et al.*, Amorphous hole-transporting layer in slot-die coated perovskite solar cells, *Nano Energy*, 2017, **31**, 210–217.
169 M. Qin, *et al.*, Perovskite solar cells based on low-temperature processed indium oxide electron selective layers, *ACS Appl. Mater. Interfaces*, 2016, **8**(13), 8460–8466.
170 K. Wang, *et al.*, Low-temperature and solution-processed amorphous $WO_x$ as electron-selective layer for perovskite solar cells, *J. Phys. Chem. Lett.*, 2015, **6**(5), 755–759.
171 D. Shen, *et al.*, Cube-like anatase $TiO_2$ mesocrystals as effective electron-transporting materials toward high-performance perovskite solar cells, *J. Colloid Interface Sci.*, 2023, **635**, 535–542.
172 W.-Q. Wu, *et al.*, Recent progress in hybrid perovskite solar cells based on n-type materials, *J. Mater. Chem. A*, 2017, **5**(21), 10092–10109.
173 X. Wang, *et al.*, Cerium oxide standing out as an electron transport layer for efficient and stable perovskite solar cells processed at low temperature, *J. Mater. Chem. A*, 2017, **5**(4), 1706–1712.
174 A. Yella, *et al.*, Nanocrystalline rutile electron extraction layer enables low-temperature solution processed perovskite photovoltaics with 13.7% efficiency, *Nano Lett.*, 2014, **14**(5), 2591–2596.
175 L. Jiang, *et al.*, Enhancing the Photovoltaic Performance of Perovskite Solar Cells with a Down-Conversion Eu-Complex, *ACS Appl. Mater. Interfaces*, 2017, **9**(32), 26958–26964.
176 S. Bhandari, *et al.*, Morphology modulated brookite $TiO_2$ and $BaSnO_3$ as alternative electron transport materials for enhanced performance of carbon perovskite solar cells, *Chem. Eng. J.*, 2022, **446**, 137378.
177 W. Tress, *et al.*, The role of the hole-transport layer in perovskite solar cells-Reducing recombination and increasing absorption, in *2014 IEEE 40th Photovoltaic Specialist Conference (PSC)*, IEEE, 2014.
178 J. Yin, *et al.*, High-Performance Inverted Perovskite Solar Devices Enabled by a Polyfullerene Electron Transporting Material, *Angew. Chem., Int. Ed.*, 2022, **61**(52), e202210610.
179 T. Leijtens, *et al.*, Overcoming ultraviolet light instability of sensitized $TiO_2$ with meso-superstructured organometal tri-halide perovskite solar cells, *Nat. Commun.*, 2013, **4**(1), 1–8.
180 W. Li, *et al.*, Enhanced UV-light stability of planar heterojunction perovskite solar cells with caesium bromide interface modification, *Energy Environ. Sci.*, 2016, **9**(2), 490–498.
181 S. Gubbala, *et al.*, Band-edge engineered hybrid structures for dye-sensitized solar cells based on $SnO_2$ nanowires, *Adv. Funct. Mater.*, 2008, **18**(16), 2411–2418.
182 Q. Zhang, *et al.*, ZnO nanostructures for dye-sensitized solar cells, *Adv. 2D Mater.*, 2009, **21**(41), 4087–4108.
183 F. Mohamadkhani, *et al.*, Improvement of planar perovskite solar cells by using solution processed $SnO_2$/CdS as electron transport layer, *Sol. Energy*, 2019, **191**, 647–653.
184 J. P. C. Baena, *et al.*, Highly efficient planar perovskite solar cells through band alignment engineering, *Energy Environ. Sci.*, 2015, **8**(10), 2928–2934.
185 H. Wang, *et al.*, Electron transport interface engineering with pyridine functionalized perylene diimide-based material for inverted perovskite solar cell, *Chem. Eng. J.*, 2022, **438**, 135410.
186 X. Zhang, *et al.*, Stable and efficient air-processed perovskite solar cells employing low-temperature processed compact $In_2O_3$ thin films as electron transport materials, *J. Alloys Compd.*, 2020, **836**, 155460.
187 C. Chen, *et al.*, Low-Temperature-Processed $WO_x$ as Electron Transfer Layer for Planar Perovskite Solar Cells Exceeding 20% Efficiency, *Solar RRL*, 2020, **4**, 1900499.
188 S. Sun, *et al.*, The origin of high efficiency in low-temperature solution-processable bilayer organometal halide hybrid solar cells, *Energy Environ. Sci.*, 2014, **7**(1), 399–407.
189 H. Li, *et al.*, Strategies for high-performance perovskite solar cells from materials, film engineering to carrier dynamics and photon management, *InfoMat*, 2022, **4**(7), e12322.
190 H. Xi, *et al.*, Performance enhancement of planar heterojunction perovskite solar cells through tuning the doping properties of hole-transporting materials, *ACS Omega*, 2017, **2**(1), 326–336.
191 Z. Xiao, *et al.*, Efficient, high yield perovskite photovoltaic devices grown by interdiffusion of solution-processed precursor stacking layers, *Energy Environ. Sci.*, 2014, **7**(8), 2619–2623.
192 K.-M. Lee, *et al.*, High-performance perovskite solar cells based on dopant-free hole-transporting material fabricated by a thermal-assisted blade-coating method with efficiency exceeding 21, *Chem. Eng. J.*, 2022, **427**, 131609.
193 H.-S. Kim and N.-G. Park, Parameters affecting *I–V* hysteresis of $CH_3NH_3PbI_3$ perovskite solar cells: effects of perovskite crystal size and mesoporous $TiO_2$ layer, *J. Phys. Chem. Lett.*, 2014, **5**(17), 2927–2934.
194 O. Malinkiewicz, *et al.*, Perovskite solar cells employing organic charge-transport layers, *Nat. Photonics*, 2014, **8**(2), 128–132.
195 A. M. Asiri, *et al.*, Solar Water Splitting Using Earth-Abundant Electrocatalysts Driven by High-Efficiency Perovskite Solar Cells, *ChemSusChem*, 2022, **15**(4), e202102471.
196 W. Sun, *et al.*, Bismuth sulfide: A high-capacity anode for sodium-ion batteries, *J. Power Sources*, 2016, **309**, 135–140.

Open Access Article. Published on 02 1402. Downloaded on 14/11/1404 12:16:38 ..
This article is licensed under a Creative Commons Attribution-NonCommercial 3.0 Unported Licence.

197 J.-H. Im, H.-S. Kim and N.-G. Park, Morphology-photovoltaic property correlation in perovskite solar cells: One-step *versus* two-step deposition of $CH_3NH_3PbI_3$, *APL Mater.*, 2014, **2**(8), 081510.

198 R. He, *et al.*, Scalable Preparation of High-Performance ZnO–$SnO_2$ Cascaded Electron Transport Layer for Efficient Perovskite Solar Modules, *Sol. RRL*, 2022, **6**(3), 2100639.

199 Z. Yan, *et al.*, Surface dipole affords high-performance carbon-based CsPbI2Br perovskite solar cells, *Chem. Eng. J.*, 2022, **433**, 134611.

200 J.-H. Im, *et al.*, Growth of $CH_3NH_3PbI_3$ cuboids with controlled size for high-efficiency perovskite solar cells, *Nat. Nanotechnol.*, 2014, **9**(11), 927–932.

201 M. Wang, *et al.*, Influence of $PbCl_2$ content in $PbI_2$ solution of DMF on the absorption, crystal phase, morphology of lead halide thin films and photovoltaic performance in planar perovskite solar cells, *J. Solid State Chem.*, 2015, **231**, 20–24.

202 M. Wang, *et al.*, A Universal Strategy of Intermolecular Exchange to Stabilize α-$FAPbI_3$ and Manage Crystal Orientation for High-Performance Humid-Air-Processed Perovskite Solar Cells, *Adv. Mater.*, 2022, **34**(23), 2200041.

203 Y. Ma, *et al.*, A highly efficient mesoscopic solar cell based on CH 3 NH 3 $PbI_{3-x}Cl_x$ fabricated *via* sequential solution deposition, *Chem. Commun.*, 2014, **50**(83), 12458–12461.

204 G. Juška, *et al.*, Extraction current transients: new method of study of charge transport in microcrystalline silicon, *Phys. Rev. Lett.*, 2000, **84**(21), 4946.

205 X. Cao, *et al.*, All green solvent engineering of organic–inorganic hybrid perovskite layer for high-performance solar cells, *Chem. Eng. J.*, 2022, **437**, 135458.

206 X. Liu, *et al.*, Chlorobenzene-Mediated Control of Crystallization in Perovskite Films for High-Performance Solar Cells, *ACS Appl. Energy Mater.*, 2020, **3**(12), 12291–12297.

207 W. Hong, *et al.*, New insights in construction of three-dimensional donor/acceptor interface for high performance perovskite solar cells: The preparation of wolf tooth stick-like $TiO_2$, *Colloids Surf., A*, 2022, **646**, 128958.

208 G. B. Adugna, S. Y. Abate and Y.-T. Tao, High-Efficiency and scalable Solution-Sheared perovskite solar cells using green solvents, *Chem. Eng. J.*, 2022, **437**, 135477.

209 N. J. Jeon, *et al.*, Solvent engineering for high-performance inorganic–organic hybrid perovskite solar cells, *Nat. Mater.*, 2014, **13**(9), 897–903.

210 Q. Liang, *et al.*, Enhancing the crystallization and optimizing the orientation of perovskite films *via* controlling nucleation dynamics, *J. Mater. Chem. A*, 2016, **4**(1), 223–232.

211 C. Zuo and L. Ding, An 80.11% FF record achieved for perovskite solar cells by using the $NH_4Cl$ additive, *Nanoscale*, 2014, **6**(17), 9935–9938.

212 M. Liu, M. B. Johnston and H. J. Snaith, Efficient planar heterojunction perovskite solar cells by vapour deposition, *Nature*, 2013, **501**(7467), 395–398.

213 Q. Chen, *et al.*, Planar heterojunction perovskite solar cells *via* vapor-assisted solution process, *J. Am. Chem. Soc.*, 2014, **136**(2), 622–625.

214 L.-C. Chen, *et al.*, Annealing effects on high-performance $CH_3NH_3PbI_3$ perovskite solar cells prepared by solution-process, *Sol. Energy*, 2015, **122**, 1047–1051.

215 A. Dualeh, N. Tétreault, T. Mohel, P. Gao, M. K. Nazeeruddin and M. Grätzel, *Adv. Funct. Mater.*, 2014, **24**, 3250–3258.

216 G. Eperon, V. Burlakov, P. Docampo, A. Goriely and H. J. Snaith, *Adv. Funct. Mater.*, 2014, **24**, 151–157.

217 L. Huang, *et al.*, Multi-step slow annealing perovskite films for high performance planar perovskite solar cells, *Sol. Energy Mater. Sol. Cells*, 2015, **141**, 377–382.

218 W. Nie, *et al.*, High-efficiency solution-processed perovskite solar cells with millimeter-scale grains, *Science*, 2015, **347**(6221), 522–525.

219 Y. Deng, *et al.*, Vividly colorful hybrid perovskite solar cells by doctor-blade coating with perovskite photonic nanostructures, *Mater. Horiz.*, 2015, **2**(6), 578–583.

220 L. A. Muscarella, *et al.*, Air-Stable and Oriented Mixed Lead Halide Perovskite (FA/MA) by the One-Step Deposition Method Using Zinc Iodide and an Alkylammonium Additive, *ACS Appl. Mater. Interfaces*, 2019, **11**(19), 17555–17562.

221 C. Wu, *et al.*, The dawn of lead-free perovskite solar cell: highly stable double perovskite $Cs_2AgBiBr_6$ film, *Adv. Sci.*, 2018, **5**(3), 1700759.

222 H. Tsai, *et al.*, Effect of precursor solution aging on the crystallinity and photovoltaic performance of perovskite solar cells, *Adv. Energy Mater.*, 2017, **7**(11), 1602159.

223 P. Boonmongkolras, *et al.*, Understanding effects of precursor solution aging in triple cation lead perovskite, *RSC Adv.*, 2018, **8**(38), 21551–21557.

224 T. H. Schloemer, *et al.*, The molybdenum oxide interface limits the high-temperature operational stability of unencapsulated perovskite solar cells, *ACS Energy Lett.*, 2020, **5**(7), 2349–2360.

225 G. Namkoong, A. A. Mamun and T. T. Ava, Impact of PCBM/C60 electron transfer layer on charge transports on ordered and disordered perovskite phases and hysteresis-free perovskite solar cells, *Org. Electron.*, 2018, **56**, 163–169.

226 K. Zhiliang, R. Yaoguang, X. Mi, L. Tongfa and H. Hongwei, Full Printable Processed Mesoscopic$CH_3NH_3PbI_3$/$TiO_2$Heterojunction Solar Cells with Carbon Counter Electrode, *Sci. Rep.*, 2013, **3**, 3132.

227 C. Qian-Qian, *et al.*, Greatly enhanced power conversion efficiency of hole-transport-layer-free perovskite solar cell *via* coherent interfaces of perovskite and carbon layers, *Nano Energy*, 2020, **77**, 10511.

228 A. Cesur, *et al.*, Tin Oxide Electron-Selective Layers for Efficient, Stable, and Scalable Perovskite Solar Cells, *Adv. Mater.*, 2021, **33**, 2005504.

229 Z. Teng, *et al.*, Improved Perovskite/Carbon Interface through Hot-Pressing: A Case Study for $CsPbBr_3$-Based Perovskite Solar Cells, *ACS Omega*, 2022, **7**(20), 16877–16883.


© 2023 The Author(s). Published by the Royal Society of Chemistry

Open Access Article. Published on 02 1402. Downloaded on 14/11/1404 12:16:38 ..
This article is licensed under a Creative Commons Attribution-NonCommercial 3.0 Unported Licence.

230 L. Siqi, *et al.*, Hole transport layer-free carbon-based perovskite solar cells with high-efficiency up to 17.49% in air: From-bottom-to-top perovskite interface modification, *Chem. Eng. J.*, 2023, **455**, 140727.
231 K. Mahmood, B. S. Swain and H. S. Jung, *Nanoscale*, 2014, **6**, 9127–9138.
232 K. Mahmood, B. S. Swain and A. Amassian, *Adv. Eng. Mater.*, 2015, **5**, 1500568.
233 K. Mahmood, B. S. Swain and A. Amassian, *Adv. Mater.*, 2015, **27**, 2859–2865.
234 Y. Semih, K. Mustafa and T. Cem, Effect of Au nanoparticle doped ZnO buffer layer on efficiency in organic solar cells, *Opt. Mater.*, 2023, **139**, 113742.
235 M. A. Tavakoli, *et al.*, A graphene/ZnO electron transfer layer together with perovskite passivation enables highly efficient and stable perovskite solar cells, *J. Mater. Chem. A*, 2019, **7**, 679–686.
236 M. A. Jalebi, *et al.*, Charge extraction *via* graded doping of hole transport layers gives highly luminescent and stable metal halide perovskite devices, *Sci. Adv.*, 2019, **5**(2), 1–9.
237 J. Zhang, *et al.*, $CsPbBr_3$ Nanocrystal Induced Bilateral Interface Modification for Efficient Planar Perovskite Solar Cells, *Adv. Sci.*, 2021, **8**, 2102648.
238 O. Elham, J. Saqib and L. Geunsik, Impact of fluorination on the energy level alignment of an $FZnP_c/MAPbI_3$ interface, *Nanoscale Adv.*, 2022, **4**, 5070–5076.

© 2023 The Author(s). Published by the Royal Society of Chemistry